

The static-exchange electron-water pseudopotential, in conjunction with a polarizable water model: A new Hamiltonian for hydrated-electron simulations

Leif D. Jacobson, Christopher F. Williams, and John M. Herbert^{a)}

Department of Chemistry, The Ohio State University, Columbus, Ohio 43210, USA

(Received 26 September 2008; accepted 6 February 2009; published online 25 March 2009)

Previously, Turi and Borgis [J. Chem. Phys. **117**, 6186 (2002)] parametrized an electron-water interaction potential, intended for use in simulations of hydrated electrons, by considering H_2O^- in the “static exchange” (essentially, frozen-core Hartree–Fock) approximation, then applying an approximate Phillips–Kleinman procedure to construct a one-electron pseudopotential representing the electron-water interaction. To date, this pseudopotential has been used exclusively in conjunction with a simple point charge water model that is parametrized for bulk water and yields poor results for small, neutral water clusters. Here, we extend upon the work of Turi and Borgis by reparametrizing the electron-water pseudopotential for use with the AMOEBA water model, which performs well for neutral clusters. The result is a one-electron model Hamiltonian for $(\text{H}_2\text{O})_n^-$, in which the one-electron wave function polarizes the water molecules, and vice versa, in a fully self-consistent fashion. The new model is fully variational and analytic energy gradients are available. We have implemented the new model using a modified Davidson algorithm to compute eigenstates, with the unpaired electron represented on a real-space grid. Comparison to *ab initio* electronic structure calculations for $(\text{H}_2\text{O})_n^-$ cluster isomers ranging from $n=2$ to $n=35$ reveals that the new model is significantly more accurate than the Turi–Borgis model, for both relative isomer energies and for vertical electron detachment energies. Electron-water polarization interactions are found to be much more significant for cavity states of the unpaired electron than for surface states. © 2009 American Institute of Physics. [DOI: 10.1063/1.3089425]

I. INTRODUCTION

The chemical physics literature is replete with electron-water interaction potentials,^{1–16} which have long been used (in conjunction with various methods of one-electron quantum mechanics) to examine the nature of the hydrated electron.^{1–32} As such, a person might reasonably question whether the chemical physics community genuinely needs yet another hydrated-electron model, especially in view of a study by Turi *et al.*¹⁰ that seems to validate certain assumptions that were made previously in the course of constructing electron-water pseudopotentials, such as the use of a local potential to model the exchange interaction. However, recent simulations³² of large $(\text{H}_2\text{O})_n^-$ clusters using the pseudopotential of Turi and Borgis,¹¹ which was parametrized for the bulk aqueous electron based upon the aforementioned analysis by Turi *et al.*,¹⁰ have failed to settle^{33–35} an old controversy regarding the nature and evolution of the electron binding motifs in finite water cluster anions, and the question of whether molecular beam experiments probe surface-bound or cavity-bound states of the unpaired electron.^{19,32–39} Thus, it appears that there is still a need for hydrated-electron models that afford quantitative results for clusters, yet are tractable enough to be used in molecular dynamics (MD) and Monte Carlo simulations, which are necessary in order to make contact with experiments.

At a phenomenological level, there are at least two important features missing from the Turi and Borgis (TB) hydrated-electron model that one might reasonably expect to be qualitatively important. The first of these is the absence of any dynamical correlation between the unpaired electron and the charge distributions of the classical water molecules, i.e., the absence of electron-water dispersion interactions. *Ab initio* electronic structure calculations demonstrate that such interactions are significantly larger for cavity-bound electrons than they are for surface-bound electrons.⁴⁰ Jordan and co-workers^{12–14,25–27} have addressed this deficiency using a quantum-mechanical Drude oscillator for each H_2O molecule,^{12,13} and this appears to be the most accurate model currently available (short of *ab initio* quantum chemistry) for prediction of vertical electron binding energies (VEBEs). Such calculations, however, require the solution of an $(n+1)$ -particle quantum mechanics problem, for a cluster of n water molecules. While far more affordable than *ab initio* calculations, the Drude model is therefore much more expensive than one-electron pseudopotential methods, and exhaustive simulations have so far been reported only for $n \leq 13$.^{13–15,27}

A second potential deficiency of the TB model, which we address here, is the use of a simple point charge (SPC) model^{41,42} for the water-water interactions. Electrostatic interactions in this model are represented by fixed, atom-centered point charges that are chosen in order to reproduce the structure of bulk water under ambient conditions. Per-

^{a)}Electronic mail: herbert@chemistry.ohio-state.edu.

haps unsurprisingly, the SPC model is rather inaccurate for predicting relative conformational energies of small neutral water clusters. Meanwhile, considerable evidence points to the fact that the neutral water potential is often more important in determining VEBEs than is the electron-water potential^{43,44} because the electron-water interaction stabilizes water networks that are extremely high in energy (and far from any stationary point) on the neutral water potential surface. Neutral water potentials, however, are rarely parametrized using such high-energy structures, and simple functional forms are not flexible enough to describe structures that are far from any local minimum. One consequence (as detailed in Refs. 43 and 44) is that small differences in the $(\text{H}_2\text{O})_n^-$ cluster geometry, which scarcely affect the total electron-water interaction energy, often substantially modify the water-water interaction and hence the VEBE, defined as

$$\text{VEBE} = E_{\text{neutral}} - E_{\text{anion}}. \quad (1)$$

Changes in the underlying water model have been shown, for example, to produce qualitatively different isomer distributions for $(\text{H}_2\text{O})_6^-$ in finite-temperature Monte Carlo simulations.²⁷

At present, the manner in which these facets of the TB model manifest as observables remains unknown. As a first step toward investigating this issue (and towards a more general investigation of the role of polarization in condensed-phase environments), we report here a reparametrization of the electron-water interaction potential, following the TB procedure but using the polarizable AMOEBA (Atomic Multipole Optimized Energetics for Biomolecular Applications) water model,⁴⁵ which is known to perform well (as judged by comparison to *ab initio* calculations) for structures and conformational energies of neutral water clusters.^{45,46} In constructing our electron-water potential, we follow the TB prescription as closely as possible so that in cases where the new model predicts different physical properties than the TB model, these differences can safely be attributed to the water-water interaction potential. The TB model reproduces the VEBE and absorption spectra in the bulk (for which it was parameterized),¹¹ and by following a similar parametrization procedure we hope to improve upon the TB model for cluster energetics while retaining accuracy in the bulk. As the TB model has been used extensively in the most recent generation of aqueous electron simulations,^{11,28–32} it serves as a *de facto* electron-water pseudopotential against which to compare the polarizable model.

The result of this work is a one-electron model Hamiltonian for $(\text{H}_2\text{O})_n^-$ in which the one-electron wave function and the classical water molecules polarize one another self-consistently. An electron-water polarization potential arises from our model in a natural way, via induced dipoles on the water molecules; the *ad hoc* polarization potential used by TB and others can be recovered as a well-defined approximation to the polarization potential arising from our model. We calculate eigenstates of the resulting one-electron Hamiltonian on a three-dimensional, real-space grid, using a modified Davidson algorithm that is considerably simpler than the Lanczos-based algorithm often used in hydrated-electron simulations.⁴⁷ Based on comparisons to *ab initio* electronic

structure calculations in $(\text{H}_2\text{O})_n^-$ clusters ($n=2–35$), the new model appears to be significantly more accurate than the TB model, for both relative conformational energies and for VEBEs.

II. BACKGROUND

A. Pseudopotential theory

To date, most electron-water pseudopotentials have been based upon the so-called static-exchange (SE) approximation.^{4,6,10,48} Within this approximation, one considers the interaction of the excess electron with the ground-state wave function of an isolated H_2O molecule. The anion's wave function is taken to be an antisymmetrized product of the excess-electron orbital and the frozen ground-state wave function of the H_2O molecule (itself an antisymmetrized product of spin orbitals), which leads to a one-electron eigenvalue equation for the excess electron,^{4,10,48}

$$\hat{H}_{\text{SE}}|\Psi\rangle = (\hat{T} + V_{\text{nuc}} + V_H + \hat{V}_x)|\Psi\rangle = \varepsilon|\Psi\rangle. \quad (2)$$

Here, \hat{T} is the one-electron kinetic energy operator, V_{nuc} is the electron-nuclear interaction, V_H is the electronic Coulomb (Hartree) potential, and \hat{V}_x is the (nonlocal) exchange operator. The quantities V_H and \hat{V}_x are identical to the Coulomb and exchange operators in a Hartree–Fock (HF) calculation of neutral H_2O , so the lowest-energy solutions of Eq. (2) are the doubly-occupied molecular orbitals (MOs) of neutral H_2O , followed by the ground-state excess-electron orbital. The highest occupied MO in the SE approximation is the lowest unoccupied MO in the HF calculation.

Although Eq. (2) is a one-electron eigenvalue equation, construction of \hat{H}_{SE} requires MOs for H_2O . This dependence must be eliminated in order to define a local potential $V(\vec{r})$ that can be fit to some analytical expression, thus converting Eq. (2) into a comparatively simple one-electron eigenvalue equation, $(\hat{T} + V)|\Psi\rangle = \varepsilon|\Psi\rangle$.

To motivate this approximation, consider the two reasons why Eq. (2) is not already such an equation: First, the nonlocality of \hat{V}_x means that the exchange interaction depends upon the core MOs; and second, the MOs must remain orthogonal (which prevents the excess electron from penetrating significantly into the core molecular region). It is common to approximate the exchange interaction with some local functional of the density, as in the electron-gas approximation,⁴⁹ which affords an attractive potential near the core region. In order to avoid collapse of the one-electron wave function into the molecule, a repulsive potential must also be included. Early pseudopotentials^{2,3,6} used a simple exponential for the repulsive potential, a functional form that can be motivated based on density-functional considerations of the change in kinetic energy upon assembling the system (e.g., H_2O^-) from its constituents ($\text{H}_2\text{O} + e^-$).⁵⁰ As an alternative, we employ a repulsive potential derived from an approximate version⁴ of the Phillips–Kleinman theory.⁵¹ This repulsive potential has the form

$$V_{\text{rep}}(\vec{r}) = - \sum_k^{\text{occupied}} \varepsilon_k \psi_k(\vec{r}) \int d\vec{r}' \psi_k(\vec{r}'), \quad (3)$$

where the ψ_k are the occupied MOs of neutral H₂O, with orbital energies ε_k .

The repulsive potential in Eq. (3) was derived from the exact Phillips–Kleinman theory by Schnitker and Rossky⁴ by expressing the wave function of the excess electron as a sum of a nodeless pseudo-wave function and a linear combination of the MOs for neutral H₂O. By subtracting out the core oscillations, one obtains a Hamiltonian that is (by construction) written for a nodeless wave function. Simplification of this Hamiltonian to yield the repulsive potential in Eq. (3) involves two assumptions:⁴ first, that the orbital eigenvalue for the excess electron is much less than the eigenvalues corresponding to core (molecular) MOs, which is validated by HF calculations; and second, that the pseudo-wave function is constant in the core region. The latter approximation was later validated by TB.¹¹

Smallwood *et al.*⁵² recently reformulated the Phillips–Kleinman treatment in a formally equivalent but computationally efficient form. We choose the approximate treatment described above so that when comparing to TB results, we may isolate (to the greatest extent possible) the effects of using a polarizable water model. The approximate Phillips–Kleinman treatment described here is used also in the Drude model of Jordan and co-workers.^{12,13}

When the repulsive potential is included in the SE Hamiltonian, the result is a Hamiltonian that contains a local pseudopotential and is easily evaluated,

$$\hat{H}_{\text{SE}}(\vec{r}) = \hat{T} + V_{\text{nuc}}(\vec{r}) + V_H(\vec{r}) + V_x[\rho(\vec{r})] + V_{\text{rep}}(\vec{r}). \quad (4)$$

Since the core MOs used to construct these local potentials are frozen, polarization is not included in the SE treatment, yet electron-water polarization is crucial to obtaining accurate VEBEs. Previous workers have dealt with this deficiency by grafting an asymptotically correct ($\propto 1r^{-4}$) polarization potential onto an otherwise nonpolarizable model,^{4,6,11} as detailed in the next section. We will instead use a polarizable water potential, from which an electron-water polarization potential arises in a natural way. Our approach is described in Sec. III.

B. TURI-BORGIS MODEL

In the model potential developed by Turi and Borgis,¹¹ the interaction between the unpaired electron and a given atomic site (oxygen or hydrogen) has a very simple functional form, expressed in terms of three error functions:

$$V_{\text{es/rep}}^{\text{TB}} = \frac{1}{r_i} \{-q^i \text{erf}(A_1^i r_i) + B_1^i [\text{erf}(B_2^i r_i) - \text{erf}(B_3^i r_i)]\}. \quad (5)$$

This potential incorporates both repulsion (rep), in the sense discussed in the previous section, as well as electrostatics (es). Beginning with Eq. (5), summation over repeated indices is implied, and atomic units are used unless otherwise specified. The quantity r_i represents the distance between the electron and the i th nucleus, the q^i are the SPC point charges, and the A_j^i and B_j^i are fitting parameters. These parameters

were not fit to reproduce the various local-potential components of the SE pseudopotential [Eq. (4)], but rather to reproduce the eigenvalue and density of the excess electron obtained by solution of Eq. (2). It is clear, however, that the first term in Eq. (5) is a damped Coulomb interaction, while the second and third terms together represent a repulsive interaction. The Coulomb potential must be damped in order to avoid singularities at the atomic sites.

The TB model predicts the optical absorption maximum of the bulk aqueous electron more accurately than previous one-electron models.¹¹ Specifically, the TB absorption maximum is redshifted relative to that predicted by previous one-electron models, which TB attribute the fact that the potential in Eq. (5) is much less repulsive at the molecular core than previous potentials, thereby allowing greater penetration of the electron into the core molecular regions.¹¹ This effect is one aspect of the TB model that we hope to retain in our reparametrization.

The polarization potential used by TB is taken from Barnett *et al.*,⁶

$$V_{\text{pol}}^{\text{TB}} = - \frac{\alpha}{2(r_{\text{oxy}}^2 + C_{\text{oxy}}^2)^2}, \quad (6)$$

where α represents the isotropic polarizability of H₂O, r_{oxy} is the electron-oxygen distance [with an implied summation over oxygen sites in Eq. (6)], and C_{oxy} is a parameter that is fit to give the correct ground-state eigenvalue of the bulk aqueous electron. This potential is spherically symmetric and has the proper r^{-4} asymptotic distance dependence, although the presence of the electron has no effect on the water-water interactions defined by the SPC water model. In this way, one might consider the TB potential to be a truly adiabatic surface, i.e., the electron-water and water-water potentials are coupled only through geometry.

Our implementation of the TB model employs the harmonic version of the flexible SPC potential,⁴² as we experienced difficulties using the Morse version of the stretching potential; see Ref. 44 for a detailed discussion. The SPC water model consists of a Coulomb interaction between point charges located at the oxygen and hydrogen sites, a 12-6 Lennard-Jones potential between the oxygen sites, and intramolecular interactions that are quadratic in the atomic displacements.

III. NEW MODEL

Our new electron-water model is based upon the polarizable water model known as AMOEBA, which is part of a more general polarizable molecular mechanics (MM) force field developed by Ren and Ponder.⁴⁵ In order to establish our notation, and to lay the groundwork for our model, we briefly review AMOEBA's electrostatic and polarization interactions in Sec. III A. (For complete details, see Ref. 45.) Following this, our electron-water model is introduced in Sec. III B.

A. AMOEBA water model

Electrostatic interactions in the AMOEBA water model are based upon electric monopole, dipole, and quadrupole

moments obtained from a distributed multipole analysis^{53,54} of gas-phase H₂O at the MP2/aug-cc-pVTZ level of theory, where MP2 denotes second-order Møller–Plesset perturbation theory. The quadrupole moments are then scaled by a factor of 0.73 in order to reproduce the “flap angle” of (H₂O)₂ predicted by *ab initio* calculations.⁴⁵

Using Applequist’s notation,^{55,56} we collect the electric multipole moments at the *i*th atomic site into a so-called polytensor,

$$\mathcal{M}_i = \begin{pmatrix} q^i \\ \vec{\mu}^i \\ \mathbf{Q}^i \end{pmatrix} \equiv [q^i, \vec{\mu}^i, \mathbf{Q}^i]^\top, \quad (7)$$

consisting of monopole (q^i), dipole (μ_α^i), and quadrupole ($Q_{\alpha\beta}^i$) moments at site *i*, where $\alpha, \beta \in \{x, y, z\}$. Throughout this work, we use curly boldface type (e.g., \mathcal{M}_i) to indicate a polytensor, whereas plain boldface type (e.g., \mathbf{Q}^i) is used for ordinary matrices. To simplify the notation, we express our formulas in terms of cartesian quadrupole moments $Q_{\alpha\beta}^i$ (following Applequist⁵⁶), whereas the AMOEBA potential (as implemented by Ren and Ponder⁴⁵ in the TINKER software package⁵⁷) employs traceless quadrupole tensors. There exists no unique transformation between a traceless quadrupole tensor and a cartesian quadrupole tensor, but the formulas presented here can be used with traceless quadrupole tensors in place of the Cartesian tensors \mathbf{Q}^i , upon scaling the latter by a factor of one-third.⁵⁸

Let us next define the multipole interaction tensor elements,

$$t^{ij} = \frac{1}{r_{ij}}, \quad (8a)$$

$$t_\alpha^{ij} = \hat{\nabla}_\alpha^i \left(\frac{1}{r_{ij}} \right), \quad (8b)$$

and

$$t_{\alpha\beta}^{ij} = \hat{\nabla}_\alpha^i \hat{\nabla}_\beta^j \left(\frac{1}{r_{ij}} \right), \quad (8c)$$

where *i* and *j* index atomic sites, $\alpha, \beta \in \{x, y, z\}$, and $r_{ij} = |\vec{r}_i - \vec{r}_j|$. From these elements we construct an interaction polytensor

$$\mathcal{T}_{ij} = \begin{pmatrix} t^{ij} & t_\alpha^{ij} & t_{\alpha\beta}^{ij} \\ -t_\alpha^{ij} & -t_{\alpha\beta}^{ij} & -t_{\alpha\beta\gamma}^{ij} \\ t_{\alpha\beta}^{ij} & t_{\alpha\beta\gamma}^{ij} & t_{\alpha\beta\gamma\delta}^{ij} \end{pmatrix}, \quad (9)$$

where the negative signs in alternating rows arise from the identity

$$\hat{\nabla}^i \left(\frac{1}{r_{ij}} \right) = -\hat{\nabla}^j \left(\frac{1}{r_{ij}} \right). \quad (10)$$

This notation enables us to write the full electrostatic potential in a simple, compact form,

$$V_{\text{es}} = \frac{1}{2} \mathcal{M}_i^\top \mathcal{T}_{ij} \mathcal{M}_j. \quad (11)$$

Equation (11) is merely a compact notation for the double Taylor series expansion of the Coulomb potential between two charge distributions; the multipole moments are the coefficients of this expansion.

In AMOEBA, polarization is represented by inducible dipoles placed at each atomic site *i*,

$$\vec{\mu}_{\text{ind}}^i = \alpha_i \vec{F}_i, \quad (12)$$

or in polytensor notation

$$\mathcal{M}_i^{\text{ind}} = \alpha_i [0, \vec{F}_i, 0]^\top \equiv \alpha_i \mathcal{F}_i, \quad (13)$$

where \vec{F}_i represents the electric field at site *i* that arises from all of the other MM sites, α_i is the isotropic polarizability at the *i*th site, and the polytensor $\mathcal{F}_i \equiv [0, \vec{F}_i, 0]^\top$ is defined for convenience. For an *N*-atom system, thus Eq. (12) represents a set of $3N$ linear equations that must be solved self-consistently for the induced dipoles (since the induced dipoles themselves contribute to the electric field).

If one writes the full multipole polytensor as the sum of permanent and induced terms, keeping in mind that only the dipoles are polarizable within the AMOEBA model, then Eq. (11) may be partitioned according to

$$V_{\text{es}} = V_{\text{es}}^{\text{perm}} + V_{\text{pol}}, \quad (14)$$

where

$$V_{\text{es}}^{\text{perm}} = \frac{1}{2} (\mathcal{M}_i^{\text{perm}})^\top \mathcal{T}_{ij} \mathcal{M}_j^{\text{perm}} \quad (15)$$

is the electrostatic interaction arising from the permanent multipoles and

$$V_{\text{pol}} = (\mathcal{M}_i^{\text{perm}})^\top \mathcal{T}_{ij} \mathcal{M}_j^{\text{ind}} + \frac{1}{2} (\mathcal{M}_i^{\text{ind}})^\top \mathcal{T}_{ij} \mathcal{M}_j^{\text{ind}} \quad (16)$$

is a polarization potential, defined as the sum of all electrostatic terms involving induced dipoles. It should also be clear that the electric field at site *i* can be generated by a polytensor \mathcal{E}_i , where

$$\mathcal{E}_i = [\phi_i, \vec{F}_i, \mathbf{G}_i]^\top = -\mathcal{T}_{ij} (\mathcal{M}_j^{\text{perm}} + \mathcal{M}_j^{\text{ind}}). \quad (17)$$

The quantities ϕ_i , \vec{F}_i , and \mathbf{G}_i are the electric potential, the electric field, and the electric field gradient at the *i*th site, respectively.

The final term that defines the electrostatic potential is the so-called self-energy,⁵⁹ i.e., the work required to distort a charge distribution from its equilibrium state (an isolated molecule) to its final state in the supramolecular system. For linear-response dipoles, the self-energy is^{55,60}

$$W_{\text{pol}} = \frac{1}{2\alpha_i} (\mathcal{M}_i^{\text{ind}})^\top \mathcal{M}_i^{\text{ind}}. \quad (18)$$

Using Eqs. (13) and (17) to simplify, and noting that

$$\mathcal{F}_i^\top \mathcal{M}_i^{\text{ind}} = \mathcal{E}_i^\top \mathcal{M}_i^{\text{ind}} \quad (19)$$

when only the dipoles are polarizable, the final expression for the electrostatic contribution to the AMOEBA water potential is

$$\begin{aligned} V_{\text{tot}} &= V_{\text{es}}^{\text{perm}} + V_{\text{pol}} + W_{\text{pol}} \\ &= \frac{1}{2} (\mathcal{M}_i^{\text{perm}})^\top \mathcal{T}_{ij} \mathcal{M}_j^{\text{perm}} + \frac{1}{2} (\mathcal{M}_i^{\text{perm}})^\top \mathcal{T}_{ij} \mathcal{M}_j^{\text{ind}}. \end{aligned} \quad (20)$$

The second equality reflects how the potential in AMOEBA is actually implemented. It should be noted that the electric field due to all atomic-site multipoles is damped using a Thole-type scheme,⁶¹ in which dipole interactions are attenuated by replacing one of the point dipoles with a smeared charge distribution. Interaction tensor elements analogous to those in Eqs. (8a)–(8c) are obtained by differentiation of the Coulomb interaction involving the smeared-out dipole. This procedure avoids the so-called polarization catastrophe, in which the electric field diverges as any site-site distance approaches zero.

Dispersion and exchange repulsion are modeled in AMOEBA using a buffered 14-7 potential.⁴⁵ Unlike SPC, AMOEBA uses pairwise van der Waals interactions at every atomic site. DeFusco *et al.*⁶² point out the necessity of including repulsive interactions between all atomic sites in order to describe the potential energy surface of the water dimer at oxygen-oxygen distances $\lesssim 2.65$ Å.

B. Electron-water potential

We are now prepared to describe the components of our electron-water potential and the fitting procedure used to parametrize it. To avoid singularities arising from the electron-water Coulomb interaction, electrostatic interactions between the electron and the water molecules must be damped. The electric field due to the electron (which is used to induce the water dipoles) must also be damped, in order to avoid a polarization catastrophe of the sort described above. The damping of both interactions is accomplished in the same manner.

In the spirit of the TB potential (and also following Staib and Borgis,⁷ who developed the first fully self-consistent model of electron-water polarization), we define a damped Coulomb potential

$$t'_{elec,j} = \frac{\text{erf}(a_j r_{elec,j})}{r_{elec,j}}, \quad (21)$$

where a_j is one of two damping parameters, one for oxygen and one for hydrogen. The subscript *elec* in this equation is a special case of the generic subscript j that indexes multipole centers. Higher-order interaction elements are derived by replacing the Coulomb potential in Eqs. (8a)–(8c) by the damped form in Eq. (21). The electric field is computed by integrating the damped analog of Eq. (8b) over the coordinates \vec{r} of the electron, weighted by the one-electron density, $|\Psi(\vec{r})|^2$.

The electron-water electrostatic interaction is

$$V_{\text{es}}^{\text{elec}} = (\mathcal{M}_{elec})^\top \mathcal{T}'_{elec,j} \mathcal{M}_j^{\text{perm}}, \quad (22)$$

where the prime indicates that the interaction matrix elements are generated from the damped Coulomb potential, Eq. (21). The polytensor \mathcal{M}_{elec} for the electron contains only a negative point charge (i.e., the dipole and quadrupole moments are set to zero), and the implied sum over j in Eq. (22) runs over all MM atoms. By defining a damped Coulomb potential, polarization from the quantum-mechanical (QM) region (i.e., the electron) arises in a natural way; we simply add the electric field due to the electron to that of the MM region when solving for induced dipoles.

In order to compute the polarization work, we separate the contributions due to the MM and QM regions. Recalling the definition of the polytensor \mathcal{F}_i in Eq. (13), we write the polarization work as

$$W_{\text{pol}} = \frac{1}{2\alpha_i} (\mathcal{M}_i^{\text{ind}})^\top \mathcal{M}_i^{\text{ind}} = \frac{1}{2} (\mathcal{F}_i^{\text{MM}} + \mathcal{F}_i^{\text{elec}})^\top \mathcal{M}_i^{\text{ind}}, \quad (23)$$

where the polytensor $\mathcal{F}_i^{\text{MM}}$ contains the electric field at site i that arises from both the permanent and induced multipoles of the MM region (\vec{F}_i^{MM}), and $\mathcal{F}_i^{\text{elec}}$ contains the electron's contribution to the electric field at the same site (\vec{F}_i^{elec}). For convenience, we define the final term in Eq. (23) to be the polarization work done by the electron,

$$W_{\text{pol}}^{\text{elec}} = \frac{1}{2} (\mathcal{F}_i^{\text{elec}})^\top \mathcal{M}_i^{\text{ind}}. \quad (24)$$

Note that while W_{pol} [Eq. (18)] is strictly positive, $W_{\text{pol}}^{\text{elec}}$ need not be. This can be understood by imagining a system in which a large electric field in the MM region effectively “wins out” over \vec{F}_i^{elec} , polarizing a dipole nearby the excess electron in such a way that this dipole has a positive (destabilizing) interaction with the electron. In such a case, $W_{\text{pol}}^{\text{elec}} < 0$, and represents a restoring force that, in the absence of the MM electric field, would re-orient the nearby dipole.

Following TB, we employ a repulsive potential of the form given in Eq. (3). This potential was computed using the MOs and orbital eigenvalues from a HF calculation of H₂O at the HF geometry. The basis set used for this calculation consists of the aug-cc-pV6Z basis with all g -type and higher angular momentum functions removed, but further augmented with two additional s -type diffuse functions on the hydrogen atoms, with exponents of 0.001 and 0.006 a.u. The integrals appearing in Eq. (3) were evaluated analytically and $V_{\text{rep}}(\vec{r})$ was calculated on a grid. These numerical data were then fit to a linear combination of four gaussian functions placed at the center of mass of the H₂O molecule.

Denoting AMOEBA's van der Waals terms and valence (intramolecular) terms as $V_{\text{disp}}^{\text{MM}}$ and $V_{\text{val}}^{\text{MM}}$, respectively, the full electron-water potential for our new model is

$$\begin{aligned} V^{\text{elec-water}} &= V_{\text{val}}^{\text{MM}} + V_{\text{disp}}^{\text{MM}} + V_{\text{es}}^{\text{MM}} + V_{\text{pol}}^{\text{MM}} + W_{\text{pol}}^{\text{MM}} + V_{\text{es}}^{\text{elec}} \\ &\quad + V_{\text{pol}}^{\text{elec}} + W_{\text{pol}}^{\text{elec}} + V_{\text{rep}}^{\text{elec}}. \end{aligned} \quad (25)$$

Writing out the electrostatic and repulsive terms explicitly, the potential is given by

TABLE I. Parameters that determine the electron-water potential developed in this work.

Parameter	Value (a.u.)
a_O	0.38
a_H	0.72
z_1	1.5
z_2	0.5
z_3	0.1
z_4	0.01
C_1	-0.0144
C_2	0.2170
C_3	0.0453
C_4	-0.0110

$$\begin{aligned}
V^{\text{elec-water}} = & V_{\text{val}}^{\text{MM}} + V_{\text{disp}}^{\text{MM}} + \frac{1}{2}(\mathcal{M}_i^{\text{perm}})^{\text{T}} \mathcal{T}_{ij} \mathcal{M}_j^{\text{perm}} \\
& + \frac{1}{2}(\mathcal{M}_i^{\text{perm}})^{\text{T}} \mathcal{T}_{ij} \mathcal{M}_j^{\text{ind}} \\
& + (\mathcal{M}_{\text{elec}})^{\text{T}} \mathcal{T}'_{\text{elec},j} \mathcal{M}_j^{\text{perm}} \\
& + (\mathcal{M}_{\text{elec}})^{\text{T}} \mathcal{T}'_{\text{elec},j} \mathcal{M}_j^{\text{ind}} + \frac{1}{2} \mathcal{M}_i^{\text{ind}} \mathcal{F}_i^{\text{elec}} \\
& + \sum_n \sum_{k=1}^4 C_k e^{-z_k R_{\text{elec},n}^2}. \quad (26)
\end{aligned}$$

The final term represents the repulsive potential, and involves a sum over each water molecule ($n=1,2,\dots$) and a second sum over four gaussians centered at that water molecule's center of mass, as discussed above. Thus $R_{\text{elec},n}$ represents the distance between the electron and the center of mass of the n th water molecule.

The new electron-water potential, Eq. (26), contains no explicit exchange potential. Exchange effects are included implicitly, as detailed in Sec. VI C, but attempts to fit exchange separately were unsuccessful. Similar difficulties were noted by TB.¹¹ Instead, we adjusted the damping parameters a_O and a_H , along with an overall scaling factor for the repulsive potential, in order to obtain an accurate VEBE for $(\text{H}_2\text{O})_2^-$. This value is the only empirical data used to parametrize our electron-water potential, and the $(\text{H}_2\text{O})_2^-$ VEBE that we obtain from the model (24 meV) is essentially the same as the MP2/6-31(1+,3+)G* value (26 meV),⁶³ which is underbound by ~ 10 meV compared to higher-level *ab initio* estimates, and by about 20 meV relative to experiment. We consider this level of accuracy acceptable. In performing the fit, we attempted to maintain the two damping parameters at similar values, in order to obtain an even-tempered electrostatic potential. The final fitted parameters are collected in Table I.

C. Polarization potential

Unlike the treatment of polarization within the TB model, the new potential, $V^{\text{elec-water}}$, includes a polarization potential, $V_{\text{pol}}^{\text{elec}} + W_{\text{pol}}^{\text{elec}}$, that arises in a natural way. We next show that the empirical polarization potential defined in Eq.

(6), and used in most previous hydrated-electron models, can be recovered as a well-defined approximation to the polarization potential in our model.

Let us momentarily ignore water-water polarization, and suppose that the induced dipoles on the MM atoms are determined solely by a point charge located at some other site that we label *elec*. Then the component of the j th induced dipole in the cartesian direction x is given by

$$\mu_{\text{ind}}^{j,x} = \alpha q^{\text{elec}} t_x^{j,\text{elec}} = -\alpha q^{\text{elec}} t_x^{\text{elec},j}. \quad (27)$$

Because we intend for the charge at site *elec* to be the unpaired electron, this equation does not contain an implicit sum over the *elec* index, nor does Eq. (28) that follows. Substituting the induced dipole in Eq. (27) into the polarization potential $V_{\text{pol}}^{\text{elec}} + W_{\text{pol}}^{\text{elec}}$, we obtain

$$V_{\text{pol}}^{\text{elec}} + W_{\text{pol}}^{\text{elec}} = -\frac{1}{2} \alpha (q^{\text{elec}} t_x^{\text{elec},j})(q^{\text{elec}} t_x^{\text{elec},j}) = -\frac{\alpha}{2r_{\text{elec},j}^4}. \quad (28)$$

Our polarization potential thus recovers the r^{-4} distance dependence of the empirical polarization potential.

In order to recover the TB polarization potential, we make a further assumption that polarization is represented not by atomic dipoles, but rather by one isotropic, inducible dipole per water molecule. Noting that the interaction tensor elements in Eq. (28) are undamped (t instead of t'), we introduce damping by replacing $r_{\text{elec},j}^2$ in this equation with $r_{\text{elec},j}^2 + C$, where C is a constant. This substitution, along with the assumption of one flexible dipole per water molecule, recovers the empirical polarization potential $V_{\text{pol}}^{\text{TB}}$ of Eq. (6). In addition to removing the singularity as $r_{\text{elec},j} \rightarrow 0$, we expect that this substitution mimics, to some extent, the effect of water-water polarization, as the bath of water molecules will tend to induce dipoles in directions dissimilar to those induced by the point charge, thus reducing the polarizing effect of the electron.

Sommerfeld *et al.*¹⁵ have provided an alternative derivation of the polarization potential, based upon an adiabatic approximation to the Drude oscillator model^{12,13} of the electron-water interaction. By averaging over the fast Drude oscillator coordinates, and expanding the electron-water interaction in powers of the electron-water distance, r , these authors obtain an asymptotic polarization potential of the form

$$V_{\text{pol}}^{\text{Drude}} = -\frac{\alpha}{2r^4} [f(r)]^2, \quad (29)$$

where $f(r)$ represents the damping function that is applied to the electron-oscillator interaction in the Drude model. Sommerfeld *et al.*¹⁵ conclude from this that the TB polarization potential implicitly includes some long-range electron-water dispersion. Note, however, that r^{-4} decay is also indicative of an ion-dipole interaction, i.e., an inductive effect, whereas (in our view) dispersion should be defined as correlation arising from electron-oscillator coupling beyond the adiabatic approximation. In our view, what Sommerfeld *et al.*¹⁵ actually proved is that the Drude oscillator model includes both dispersion and polarization.

D. Energy gradients

Gradients of the electron-water potential are formally simple due to the variational nature of the model. A single-point energy calculation minimizes the total energy with respect to all parameters in the Hamiltonian, namely, the induced dipoles for the MM atoms, and the expansion coefficients of the one-electron wave function (grid amplitudes, in our implementation). Stationarity with respect to the latter is obvious since the wave function is determined by solving the equation $\hat{H}|\Psi\rangle = E|\Psi\rangle$, where

$$\hat{H} = \hat{T} + V^{\text{elec-water}} + V^{\text{AMOEB A}}. \quad (30)$$

However, the induced dipoles that determine \hat{H} are themselves determined by solution of the coupled linear equations represented by Eq. (12), and it is not immediately obvious that these parameters are indeed variational. This we now demonstrate, following the proof outlined in Ref. 64.

One may imagine determining the one-electron wave function via a minimization carried out in two separate steps. First, we fix the induced dipoles and minimize the expectation value of the Hamiltonian with respect to linear expansion coefficients of the wave function (grid amplitudes). This minimization is equivalent to solving $\hat{H}|\Psi\rangle = E|\Psi\rangle$, and yields a new one-electron density and hence a new electric field, \vec{F}_i^{elec} , at each MM site i . This electric field, together with that of the water molecules, is then used to compute the induced dipoles, and the energy (at fixed values of the wave function coefficients) may be expressed as a function of these dipoles,

$$\begin{aligned} E(\mathcal{M}^{\text{ind}}) &= \frac{1}{2} \mathcal{M}_i^\top \mathcal{T}_{ij} \mathcal{M}_j \\ &+ \langle \Psi | (\mathcal{M}_{\text{elec}})^\top \mathcal{T}_{\text{elec},j} \mathcal{M}_j^{\text{ind}} | \Psi \rangle \\ &+ \frac{1}{2\alpha_i} (\mathcal{M}_i^{\text{ind}})^\top \mathcal{M}_i^{\text{ind}}. \end{aligned} \quad (31)$$

The second step is to minimize the function $E(\mathcal{M}^{\text{ind}})$ with respect to the induced dipoles. Taking the derivative of Eq. (31) with respect to the induced dipole on the k th site, $\partial E / \partial \vec{\mu}_{\text{ind}}^k$, and equating the result to zero, one obtains

$$\begin{aligned} 0 &= \mathcal{T}_{ki} \mathcal{M}_i + \langle \Psi | \mathcal{T}_{k,\text{elec}} \mathcal{M}_{\text{elec}} | \Psi \rangle + \frac{1}{\alpha_k} \mathcal{M}_k^{\text{ind}} \\ &= -\mathcal{E}_k^{\text{MM}} - \mathcal{E}_k^{\text{elec}} + \frac{1}{\alpha_k} \mathcal{M}_k^{\text{ind}}. \end{aligned} \quad (32)$$

Since only the dipoles are inducible in our model, this last expression simplifies to

$$0 = -\vec{F}_k^{\text{MM}} - \vec{F}_k^{\text{elec}} + \alpha_k^{-1} \vec{\mu}_{\text{ind}}^k, \quad (33)$$

which shows that the variational condition $\partial E / \partial \vec{\mu}_{\text{ind}}^k = 0$ is equivalent to Eq. (12), the equation that determines the linear-response dipoles. Thus, gradients of the energy require only direct differentiation of the Hamiltonian, i.e., Hellman-Feynman forces, with no response terms.

The variational nature of our hydrated-electron model stands in contrast to the polarizable models developed re-

cently by Sommerfield and co-workers.^{14,15} These authors do not include $\mathcal{E}_k^{\text{elec}}$ in the field that polarizes the water molecules (i.e., the water molecules polarize one another, and they polarize the one-electron wave function, but the wave function does not polarize the water molecules). Consequently, the energy is not variational with respect to the induced dipoles, so calculation of the gradients requires the solution of linear equations that determine how the induced dipoles respond to the perturbation.⁶⁵ This procedure is adopted, we presume, in anticipation of using these potentials in conjunction with a Drude oscillator model that would replace the electron-water (but not the water-water) polarization interactions, as has been done in previous Drude oscillator models developed by Jordan and co-workers.^{12,13} Nevertheless, such an approach does lack the desirable features of self-consistency and satisfaction of a variational theorem.

IV. SIMULATION ALGORITHM

This section describes the algorithm that we employ to calculate eigenstates of the one-electron model Hamiltonian, Eq. (30). Because analytic energy gradients are available, this algorithm may equally well be used to perform quantum/classical MD simulations, in which classical MD for the water molecules is propagated on the adiabatic potential energy surface corresponding to some eigenvalue of \hat{H} , but always with self-consistent polarization of the wave function and the water molecules.

We calculate the lowest few eigenstates of \hat{H} on an evenly spaced cartesian grid in three dimensions,^{66,67} via an iterative technique described below, then calculate forces on the atoms via the Hellmann-Feynman theorem, $\partial E / \partial x = \langle \Psi | \partial V / \partial x | \Psi \rangle$. Regarding iterative eigensolvers, Webster *et al.*⁴⁷ note that Lanczos-type methods are problematic for hydrated-electron models due to the high spectral density of \hat{H} . This problem is especially severe for clusters, which may possess no more than a few bound states. We are consistently able to converge the ground state, and occasionally one or two excited states, using a standard block-Lanczos procedure, but we are unable to converge all of the excited states that have significant oscillator strength out of the ground state.

To overcome this problem, Webster *et al.*⁴⁷ employed a two-step procedure that involves first using Lanczos iteration to determine eigenpairs of the operator

$$\hat{H}_\lambda = \exp(-\lambda V/2) \exp(-\lambda \hat{T}) \exp(-\lambda V/2), \quad (34)$$

where $\hat{H} = \hat{T} + V$ is the original Hamiltonian. If the parameter $\lambda > 0$ is sufficiently large, then the spectrum of \hat{H}_λ will be much less dense than that of \hat{H} , making the former amenable to Lanczos iteration. A second Lanczos procedure is then used to correct for the fact that the eigenstates of \hat{H}_λ are not eigenstates of \hat{H} . When using this technique, one must take steps to detect and remove spurious eigenvalues.^{47,68}

As an alternative to this rather complicated prescription (which appears still to be in use^{11,22,32}), we calculate eigenstates of \hat{H} via block-Davidson iteration,⁶⁹ a procedure that is known to work well for diagonally dominant matrices. When

represented on a real-space grid, the matrix of V is strictly diagonal, while the matrix representation of \hat{T} decays quadratically away from the diagonal,⁶⁷

$$T_{ij} = \frac{(-1)^{i-j} \hbar^2}{2m(\Delta x)^2} \begin{cases} \frac{1}{3} \pi^2, & i=j \\ 2(i-j)^{-2}, & i \neq j. \end{cases} \quad (35)$$

For fixed-charge potentials (e.g., the TB model), we employ a standard version of the Davidson algorithm (as described, for example, in the Appendix of Ref. 70). All subspace vectors $\mathbf{v}_1, \mathbf{v}_2, \dots, \mathbf{v}_N$ are stored in core memory, as are the vectors $\mathbf{w}_i = \mathbf{H}\mathbf{v}_i$ generated by the action of Hamiltonian matrix. Some limited testing led us to cap the number of subspace vectors at $N \sim 200$ to avoid a diagonalization bottleneck; if the subspace size reaches this limit, it is collapsed down to one vector per desired root. We employ a “locking” procedure, whereby only the unconverged roots are used to generate new subspace vectors.⁷⁰

Comparison to exact diagonalization indicates that this procedure consistently determines as many eigenpairs of \hat{H} as desired, to arbitrary accuracy and without spurious eigenvalues. Starting from guess vectors with random entries, with a limit of $N=200$ subspace vectors and a very stringent convergence criterion ($\|(\hat{H}-E)\Psi\| < 1.0 \times 10^{-8}$ a.u.), the subspace must be collapsed two or three times in order to calculate the lowest five eigenstates of a $(\text{H}_2\text{O})_{216}^-$ cluster in which the electron is contained within a cavity. (For the TB model, these five states account for $\geq 90\%$ of the oscillator strength from the ground state.) For geometry optimizations and MD simulations, where converged eigenvectors from a previous step are available as an initial guess, the same calculation requires only 15–25 subspace vectors per root, for MD, and significantly fewer than that for geometry optimizations. In fact, for geometry optimizations it is often the case that *zero* additional subspace vectors are required, i.e., it is only necessary to diagonalize the new Hamiltonian in the basis of converged eigenvectors from the previous geometry. (To some extent, this is a consequence of the fact that we optimize in cartesian coordinates, where the step sizes are necessarily small.)

The simple block-Davidson procedure must be modified for polarizable water models, because in this case \hat{H} depends upon the values of the induced dipoles. These in turn depend upon the one-electron density, $|\Psi(\vec{r})|^2$, and thus \hat{H} is a functional of its own eigenvectors. Strictly speaking, the vectors \mathbf{w}_i therefore become out of date every time one adds a new subspace vector because each new subspace vector modifies the approximate eigenvectors (Ritz vectors), thus altering the density $|\Psi(\vec{r})|^2$ that is used to polarize the water molecules, and consequently modifying the Hamiltonian itself. However, the difference in $\mathbf{w}_i = \mathbf{H}\mathbf{v}_i$ is typically quite small from one iteration to the next, especially in the later iterations.

The procedure that we adopt is to update the subspace matrix every time that the norm of the residual vector decreases by a factor of 2–5. We store the potential energy vector each time that we polarize the water molecules with the electron density; once we decide to update, we repolarize

the solvent bath, compute the change ΔV in the potential energy at each grid point, and finally update the matrix-vector products \mathbf{w}_i using ΔV . This procedure is very efficient for smaller clusters with highly diffuse, surface-bound electrons, where a large grid is required but where the potential and linear-response equations [Eq. (12)] are inexpensive to compute. All results presented here utilize this algorithm.

Preliminary calculations on larger clusters [e.g., $(\text{H}_2\text{O})_{216}^-$] that exhibit cavity-bound electrons indicate that high accuracy can be achieved using much smaller grids since the electron is highly localized, but that evaluation of the potential and self-consistent iteration for the induced dipoles are the bottleneck steps. (In smaller clusters with large grids, repeated formation of matrix-vector products is the most expensive step.) For these larger clusters, it is advantageous to converge all eigenvectors of interest between each update of the dipoles. Overall convergence is achieved when the difference in energy between updates of the dipoles is smaller than some threshold, for each eigenvalue of interest. This typically requires three to five updates of the dipoles for an energy threshold of 10^{-6} a.u.

V. COMPUTATIONAL DETAILS

Grid-based model Hamiltonian calculations were performed with our homebuilt Fourier grid code, FURRY (version A), which incorporates a locally modified version of the TINKER MM software (Ref. 57) to evaluate the AMOEBA water potential, solve for the induced dipoles, and evaluate the electron-water potential. All *ab initio* calculations were performed using a locally modified version of Q-CHEM,⁷¹ in which we have implemented^{72,73} the long-range-corrected (LRC)-BOP density functional that is discussed below. The remainder of this section provides details of both the Fourier grid calculations and the *ab initio* benchmarks.

All eigenpairs were converged to an accuracy of $\|(\hat{H}-E)\Psi\| < 10^{-6}$ a.u. Our calculations employ a $60 \times 60 \times 60 \text{ \AA}^3$ cartesian grid with a spacing of $\Delta x = 1.0 \text{ \AA}$, except in the case of $(\text{H}_2\text{O})_2^-$, where an 80 \AA wide cubic grid (with the same Δx) is necessary to converge the ground-state eigenvalue with respect to the grid parameters. Geometry optimizations were performed with a smaller $40 \times 40 \times 40 \text{ \AA}^3$ grid, again with $\Delta x = 1.0 \text{ \AA}$. Note that the maximum momentum component in the x direction is $\hbar \pi / \Delta x$,⁷⁴ thus the maximum kinetic energy of the wave function is $(3/2m) \times (h\pi/\Delta x)^2$. Values for $\langle \hat{T} \rangle$ in our calculations are well below this upper bound. Furthermore, numerical tests reveal that VEBEs obtained using the aforementioned grids are converged to within 0.01–0.02 eV of the $\Delta x \rightarrow 0$ limit. At this level, the magnitude of the grid truncation error is smaller than the intrinsic accuracy of the calculated VEBEs themselves.

In Sec. VI, we validate the accuracy of predicted VEBEs against benchmark *ab initio* calculations, using a library of 92 $(\text{H}_2\text{O})_n^-$ cluster isomers that we have assembled from our previous work,^{40,75} which range in size from $n=2$ to $n=35$, including both surface and cavity electron binding motifs, and with VEBEs ranging from ≈ 0 up to 2.5 eV. Atomic coordinates for these structures, along with energies calcu-

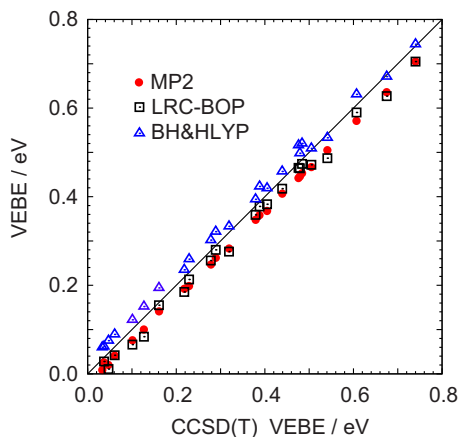


FIG. 1. (Color online) Comparison of VEBEs obtained with various *ab initio* methods to those obtained at the CCSD(T) level, for a set of 24 $(\text{H}_2\text{O})_n^-$ cluster isomers ranging from $n=2$ to $n=7$, each of which is a stationary point at the B3LYP/6-31(1+,3+)G* level. The MP2 and CCSD(T) calculations employ the 6-31(1+,3+)G* basis set, while the density-functional calculations use the aug-cc-pVDZ+diff basis. LRC-BOP calculations employ a range-separation parameter of 0.33 bohr⁻¹, as recommended in Ref. 76. The diagonal line indicates where the predicted VEBE is the same as the CCSD(T) value.

lated at various levels of theory, are available in the supporting information.

We have made extensive use of the MP2/6-31(1+,3+)G* method for *ab initio* VEBE predictions,^{40,43,63,75} as this approach typically affords VEBEs that lie only ~ 30 meV below accurate CCSD(T) values,^{63,75} yet is affordable enough to be applied to the $(\text{H}_2\text{O})_n^-$ clusters in our database. Recently, however, Yagi *et al.*⁷⁶ demonstrated that the LRC-BOP functional,^{77,78} which asymptotically incorporates full HF exchange, affords VEBEs of comparable or slightly better quality than MP2/6-31(1+,3+)G* values. (This stands in sharp contrast to most traditional density functionals, which significantly overestimate VEBEs.⁶³) As such, we will compare MP2 and LRC-BOP results, in order to ascertain whether a more reliable set of VEBE benchmarks can be obtained. We will also compare to results obtained with the BH&HLYP functional,⁷⁹ as this functional performs well for electron affinities.⁸⁰

For all density-functional calculations, we employ the basis recommended by Yagi *et al.*,⁷⁶ which we denote as aug-cc-pVDZ+diff. Relative to aug-cc-pVDZ, this basis is further augmented with an additional diffuse *s* function on each hydrogen atom (with an exponent of 3.72×10^{-2} a.u.) as well as a diffuse *s* function and a set of diffuse *p* functions on each oxygen atom (with exponents of 9.87×10^{-2} and 8.57×10^{-2} a.u., respectively).

Figure 1 shows that VEBEs calculated with either LRC-BOP or BH&HLYP are quite comparable to MP2/6-31(1+,3+)G* results. The mean absolute errors [relative to CCSD(T)/6-31(1+,3+)G* values] are 30 ± 6 meV for MP2, 25 ± 13 meV for LRC-BOP, and 22 ± 10 meV for BH&HLYP, where error bars indicate one standard deviation. (For comparison, the B3LYP error is 194 ± 36 meV, always in the direction of overbinding. The smaller amount of HF exchange in this functional leads to significant self-interaction associated with the singly-occupied MO, leading

to overstabilization of the anion.) In our calculations, MP2 exhibits the most systematic error, although this was not observed by Yagi *et al.*⁷⁶ and may result from the fact that our MP2 and CCSD(T) calculations both employ the same (rather small) basis set.

For the entire database of 92 cluster isomers (with VEBEs ranging up to 2.5 eV), the mean absolute deviation from MP2 is 37 meV for LRC-BOP and 51 meV for BH&HLYP, although the latter functional exhibits several outliers that differ by ~ 0.2 eV from the MP2 and LRC-BOP values. We will therefore use the MP2/6-31(1+,3+)G* and LRC-BOP/aug-cc-pVDZ+diff levels of theory to benchmark VEBEs. The mean *signed* deviation between the VEBEs calculated by these two methods is only 17 meV.

In Sec. VI we will also test the accuracy of the model Hamiltonians for predicting relative conformational energies of small clusters. As conformational energies place more stringent demands on the basis set, for these quantities we benchmark against MP2 energies extrapolated to the complete basis set (CBS) limit. The MP2/CBS energies were determined by separate extrapolation of the HF energy and the MP2 correlation energy, using the aug-cc-pVXZ+diff sequence of basis sets, where $X=2, 3$, or 4 (i.e., D, T, or Q) and “+diff” signifies the addition of extra diffuse functions, as specified above. (The same set of additional diffuse functions was used for each X .) The HF/CBS energy was estimated using a three-point fit to the *ansatz*⁸¹

$$E(X) = E(\infty) + ae^{-bX}, \quad (36)$$

where a and b are fitting parameters. The MP2 correlation energy was extrapolated using a two-point fit ($X=3$ and 4) to the expression⁸²

$$E(\infty) = E(X) + cX^{-3}, \quad (37)$$

where c is a fitting parameter.

VI. ANALYSIS OF THE NEW MODEL

We now turn our attention from the development and technical description of the model to the analysis of its properties. We first verify, by comparison to *ab initio* benchmarks, that the new model Hamiltonian is indeed more accurate than the TB model for $(\text{H}_2\text{O})_n^-$ clusters. We then make a detailed analysis of the potential itself, in order to compare and contrast it with the TB potential. In this work, we consider only the ground state of the model potentials.

A. VEBEs

Figure 2 compares MP2 VEBEs to those obtained from the two model Hamiltonians, for 91 different $(\text{H}_2\text{O})_n^-$ isomers ranging from $n=3$ to $n=35$. Overall, our new model outperforms the TB model, reducing the mean absolute deviation (with respect to the MP2 values) from 263 ± 185 to 108 ± 89 meV. The maximum deviation is also reduced, from 744 meV (TB model) to 348 meV (new model). We emphasize that our model is fit exclusively to the VEBE of $(\text{H}_2\text{O})_2^-$, so we regard the rather small errors in VEBEs as evidence that our model contains most of the correct physics for $(\text{H}_2\text{O})_n^-$. (As discussed below, a QM treat-

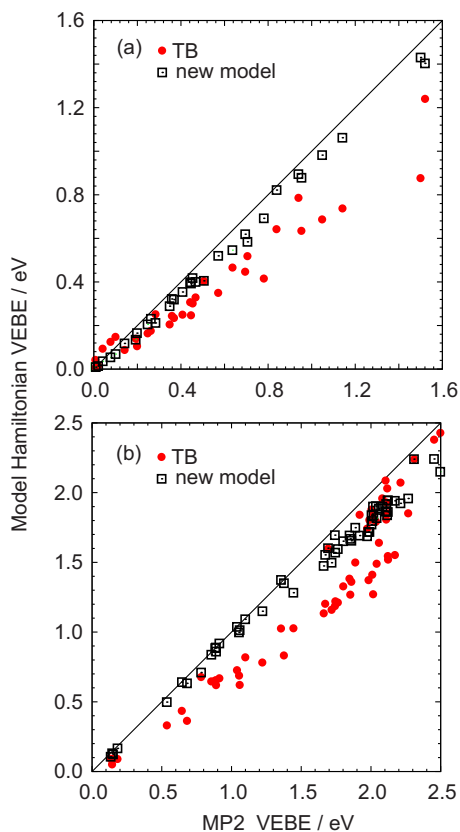


FIG. 2. (Color online) Comparison of VEBEs computed at the MP2/6-31(1+,3+)G* level of theory to those predicted using model Hamiltonians, for (a) 32 $(\text{H}_2\text{O})_n^-$ isomers ranging from $n=3$ to $n=19$, and (b) 59 $(\text{H}_2\text{O})_n^-$ isomers ranging from $n=20$ to $n=35$. The diagonal line indicates where the model Hamiltonian and MP2 predictions are identical.

ment of electron-water dispersion, which is absent or at best implicit in our model, affords VEBEs that are even more accurate.) By fitting our potential to a subset consisting of 20 out of the 92 VEBE data points, we can reduce the mean error for the entire database to 58 meV; in the present work, however, we opt to use the potential that is fit only to $(\text{H}_2\text{O})_2^-$.

Turi *et al.*³² suggest that the TB model is expected to give large errors for clusters smaller than $n=20$, so in Fig. 2 we have segregated the VEBEs based upon this size criterion. For the TB model, the mean absolute deviations from MP2 are 167 ± 106 meV for $n < 20$ and 318 ± 189 meV for $n > 20$. Apparently, errors in the TB binding energy predictions are not strictly related to cluster size. Our new model is more accurate than TB in both size categories, with mean absolute deviations of 53 ± 30 meV ($n < 20$) and 139 ± 97 meV ($n > 20$). For the $n > 20$ clusters, the mean error in both models would decrease by about 30 meV if we took the LRC-BOP values as benchmarks, rather than the MP2 values.

The cluster geometries in our database were obtained in a variety of ways. All but six of the $n < 20$ geometries in Fig. 2(a) were taken from Ref. 75, where they were optimized at the B3LYP/6-31(1+,3+)G* level. The remaining six of these smaller clusters, and all of the larger clusters, were taken from an equilibrated MD simulation of a $(\text{H}_2\text{O})_{216}^-$ cavity state at $T=150$ K, as described by the TB model

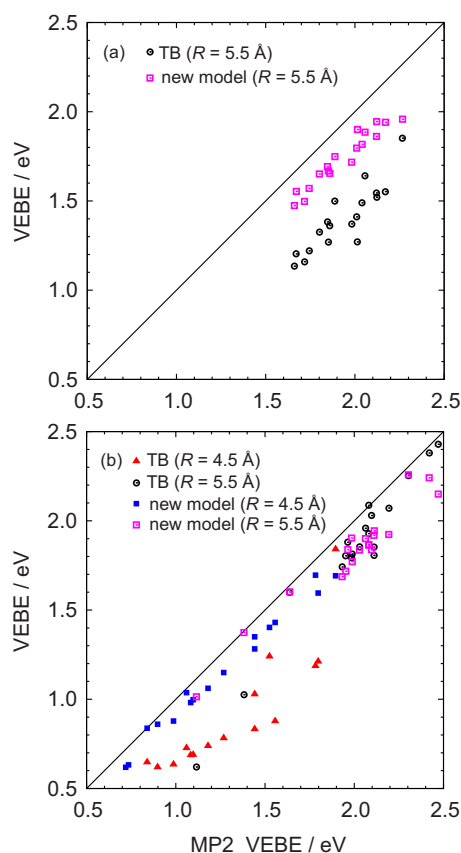


FIG. 3. (Color online) Comparison of VEBEs computed at the MP2/6-31(1+,3+)G* level of theory to those predicted using model Hamiltonians, for $(\text{H}_2\text{O})_n^-$ isomers (with $17 \leq n \leq 35$) that were (a) extracted from a MD simulation, as described in the text; and (b) subsequently optimized, using the TB model.

Hamiltonian.⁴⁰ Clusters were extracted from this simulation at 1 ps intervals, by selecting all water molecules within either $R=4.5$ Å or $R=5.5$ Å of the centroid of the wave function, radii that were dictated by the size constraints of the subsequent MP2 calculations. The number of monomers in the $R=4.5$ Å clusters ranges from $n=17$ to $n=24$, which is insufficient to complete the electron's first solvation shell. As such, these clusters are not really representative of either the bulk environment or stable cluster structures, so we subsequently optimized the geometries on the TB potential surface. Only the optimized structures were placed into the database. The larger ($R=5.5$ Å) clusters, on the other hand, each contain 30–35 water molecules, enough to complete one solvation shell. We include these clusters in the database both before and after optimization on the TB potential surface.

Figure 3 breaks down the VEBE predictions among the three sets of isomers obtained from the simulation (i.e., $R=4.5$ Å, optimized; $R=5.5$ Å, optimized; and $R=5.5$ Å, unoptimized). For the TB model, optimization of the 5.5 Å clusters significantly improves the accuracy of the predicted VEBEs, reducing the mean absolute deviation (relative to MP2) from 744 to 166 meV, whereas the optimized 4.5 Å clusters exhibit a mean error of 373 meV. The performance of our new model, in contrast, is not strongly affected by optimization. (In particular, the mean error is virtually un-

changed.) We take this as compelling evidence that our new hydrated-electron model provides a more uniform description of the global $(\text{H}_2\text{O})_n^-$ potential energy surface, including both surface states and cavity states.

Focusing on the $R=5.5$ Å clusters, we note that VEBEs predicted by the new model track the MP2 results fairly well, regardless of whether the cluster structures are optimized or simply carved out of the MD simulation. (Note that both the MD simulation and the subsequent geometry optimizations were performed using the TB model Hamiltonian.) In contrast, the accuracy of the TB model improves significantly upon geometry optimization, to the point where (for optimized clusters) the accuracy is comparable to that of the new model, and slightly better for those structures exhibiting the largest VEBEs. (Note that the TB model was parameterized using bulk aqueous electron data,¹¹ for which the experimental VEBE is estimated to be ≈ 3.3 eV,^{36,83} whereas our model is parameterized using the VEBE of the gas-phase water dimer anion, which is measured to be 0.045 eV.³⁶) Presumably, optimization restores the clusters to more bulk-like structures, for which the TB model performs well. In future simulations, we plan to evaluate the performance of our model for the bulk aqueous electron.

Finally, it is significant that our model underbinds the electron in nearly all cases. We have neglected a QM treatment of electron-water dispersion, a correct description of which would probably increase the calculated VEBEs.¹⁵ Using a Drude model to incorporate this interaction, Wang and Jordan¹² report errors of less than 5 meV in small-cluster VEBEs ($n \leq 4$), relative to CCSD(T) benchmarks. This suggests a hierarchy of model Hamiltonians of increasing complexity, expense, and accuracy. A nonpolarizable water model combined with an asymptotically correct polarization potential suffices to predict VEBEs within ~ 0.3 eV (albeit with some fairly significant outliers), while a self-consistent treatment of polarization decreases this error to about 0.1 eV and renders it much more systematic. A QM description of dispersion reduces the error even further, at significantly greater computational expense.

B. Conformational energies

Another important test of a model potential is its ability to predict relative conformational energies of cluster isomers. In the case of $(\text{H}_2\text{O})_n^-$ clusters, molecular beam experiments appear to sample preferentially those isomers with the largest VEBEs,⁸⁴ which tend to be fairly high-energy local minima on the anion potential energy surface.⁴³ For this reason, we desire a model that can predict relative conformational energies, for both $(\text{H}_2\text{O})_n$ and $(\text{H}_2\text{O})_n^-$ cluster isomers, at energies well above the global minimum. Thus, we next compare the relative conformational energies predicted by the model Hamiltonians to those obtained at the MP2/CBS level, for a set of $(\text{H}_2\text{O})_4^-$, $(\text{H}_2\text{O})_5^-$, and $(\text{H}_2\text{O})_6^-$ cluster isomers whose structures are depicted in Fig. 4. Each isomer in Fig. 4 is a stationary point at the B3LYP/6-31(1+,3+)G* level of theory, and the MP2/CBS energy calculations use these B3LYP geometries. For the model Hamiltonian calculations, the B3LYP geometries were re-optimized using the In

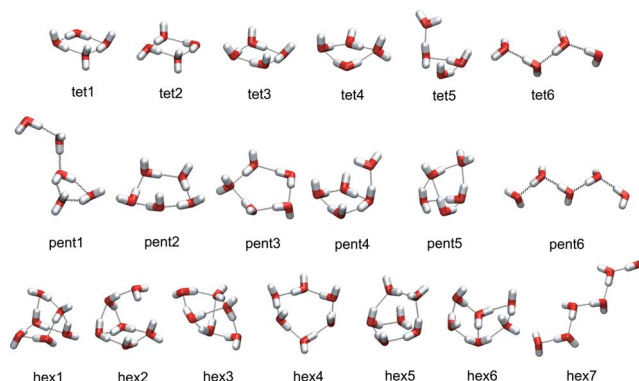


FIG. 4. (Color online) Structures of the $(\text{H}_2\text{O})_4^-$, $(\text{H}_2\text{O})_5^-$, and $(\text{H}_2\text{O})_6^-$ isomers used to benchmark relative conformational energies. Each geometry shown here is a stationary point at the B3LYP/6-31(1+,3+)G* level.

what follows, we discuss relative conformational energies, not only for these anionic clusters but also for the corresponding neutral cluster isomers computed at the anion geometries.

Figure 5 compares the relative conformational energies for the tetrameric clusters. Five of the six structures exhibit the well-known “double acceptor” or AA structural motif,^{43,85} in which one of the water molecules accepts two hydrogen bonds and donates none, leaving it with two “dangling” hydrogen atoms. The excess-electron wave function (or singly-occupied MO, in the case of *ab initio* calculations) is largely localized around this AA water molecule. Among these six cluster isomers, the only non-AA isomer is the cyclic structure tet3 (see Fig. 4), which represents the lowest-energy structure (of those considered here) on both the anionic and the neutral potential energy surfaces. [In view of the extensive *ab initio* calculations available for the tetramer,^{43,86} it seems safe to conclude that tet3 is the global minimum of $(\text{H}_2\text{O})_4^-$. This isomer is structurally similar to

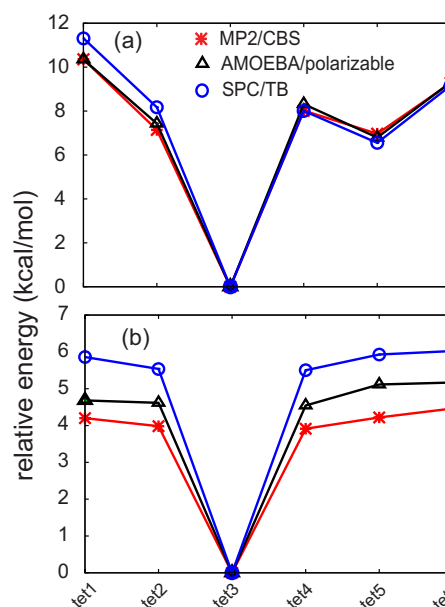


FIG. 5. (Color online) Energies of tetrameric clusters on (a) the $(\text{H}_2\text{O})_4$ potential surface and (b) the $(\text{H}_2\text{O})_4^-$ potential surface. Note that the two panels use different energy scales. *Ab initio* geometries for each cluster are depicted in Fig. 4.

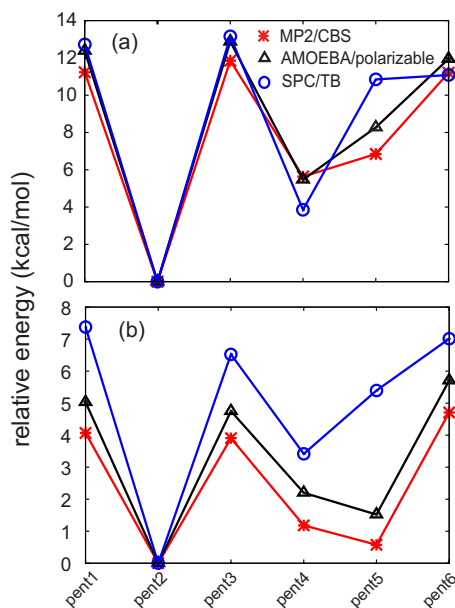


FIG. 6. (Color online) Energies of pentameric clusters on (a) the $(\text{H}_2\text{O})_5$ potential surface and (b) the $(\text{H}_2\text{O})_5^-$ potential surface. Note that the two panels use different energy scales. *Ab initio* geometries for each cluster are depicted in Fig. 4.

the $(\text{H}_2\text{O})_4$ global minimum.^{43]} The AA isomers, although they are far more prominent in the experimental photoelectron spectrum of $(\text{H}_2\text{O})_4^-$,⁸⁷ each lie at least 4 kcal/mol above tet3; upon detachment of the excess electron, these AA structures lie at least 8 kcal/mol above the neutral tet3 isomer.

The SPC and TB models perform remarkably well at describing the relative energies of the $(\text{H}_2\text{O})_4$ isomers, which is somewhat surprising in view of the fact that both models were parametrized for the bulk. For the neutral tetramers, the largest difference between MP2/CBS and SPC is only about 1.0 kcal/mol, versus 0.3 kcal/mol for AMOEBA. Both anion models overstabilize the tet3 isomer, although the largest error for our model is only 0.9 kcal/mol, versus 1.7 kcal/mol for the TB model.

Like the tetramers, the pentameric structures are mostly AA-type binding motifs, the exception being the neutral-like pent2 isomer (see Fig. 4). Relative energies of these isomers are depicted in Fig. 6, and once again the non-AA isomer is the lowest-energy structure on both the neutral and the anionic potential surface. Looking at the $(\text{H}_2\text{O})_5^-$ relative energies, the largest difference between the MP2/CBS and the TB results occurs for isomer pent5, coinciding with the largest differences between SPC and MP2/CBS for the neutral pentamers. The AMOEBA water model once again agrees *quantitatively* with MP2/CBS results for the neutral pentamer structures. Relative energies of $(\text{H}_2\text{O})_5^-$ isomers, as predicted by our new model, agree with MP2/CBS results to within 1 kcal/mol.

Stationary points for the $(\text{H}_2\text{O})_5^-$ clusters on the TB surface are compared to the corresponding B3LYP/6-31(1+,3+)G* geometries in Fig. 7. (With regard to the analysis that follows, similar arguments can be made for the hexamers.) Geometries optimized using our new model Hamiltonian are nearly identical to the B3LYP structures, and are therefore omitted. The TB model (and underlying SPC

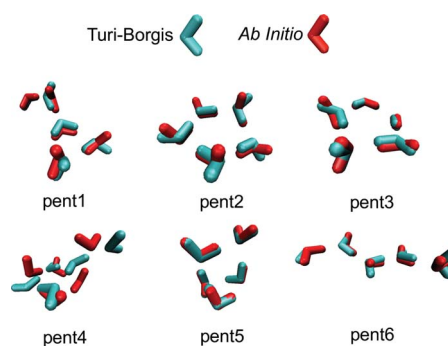


FIG. 7. (Color online) Stationary points of $(\text{H}_2\text{O})_5^-$ isomers on the TB potential surface compared to stationary points at the B3LYP/6-31(1+,3+)G* level.

model) tends to produce geometries in which the water molecules lie in a plane, as seen for example in structure pent2, where the hydrogen atoms not involved in hydrogen bonding tend to point directly away from the center of the ringlike network of hydrogen bonds. This is not observed in the corresponding B3LYP geometry. Another striking example is pent4, where reoptimization of the B3LYP geometry using the TB model causes the structure to collapse to something that is nearly planar. The reason for this behavior is fairly clear: within the SPC model, the minimum-energy geometry tends to align the dipoles created by the fixed point charges, resulting in overly planar clusters. The new model is free of this artifact, owing to the presence of electrical quadrupole moments, the first multipole moments in H_2O that have out-of-plane components. Tellingly, the only pentamer for which TB/SPC does not significantly exaggerate the planarity is isomer pent5, for which alignment of the dipoles would break hydrogen bonds. This geometry can be thought of as “strained” on the TB potential surface, and as a result it lies quite high in energy, despite the fact that it has more hydrogen bonds than the other pentamers considered here.

Each of the tetrameric geometries in our data set can accommodate some alignment of dipoles without breaking any hydrogen bonds, so the TB model performs rather well for these clusters, as evident from Fig. 5. In contrast, many of the hexamer geometries do not allow such alignment, and we will see that the TB model performs rather poorly for these isomers. We suspect that any water model that relies solely on point charges at atomic centers to describe electrostatic interactions will suffer from this planarity problem, and that only models with explicit quadrupole interactions will accurately describe cluster geometries.

Relative energies for the hexameric clusters are depicted in Fig. 8. For the neutral hexamers, SPC is unsatisfactory while the AMOEBA potential performs well, aside from one isomer (hex2) that is omitted from Fig. 8, for reasons discussed below. For the hexamer anions, the TB model predicts three isomers below the correct minimum-energy structure (the AA isomer hex5). The correct minimum-energy structure is one that we suspect to be strained on the TB/SPC potential surface, in the sense described above, and should actually lie much lower in energy. Our new model also predicts one isomer (hex3) to be lower in energy than the *ab initio* minimum, although only by 0.3 kcal/mol. The TB

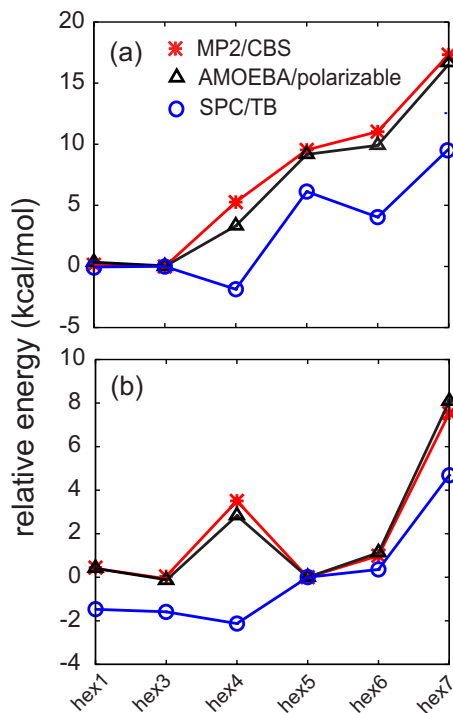


FIG. 8. (Color online) Energies of hexameric clusters on (a) the $(\text{H}_2\text{O})_6$ potential surface and (b) the $(\text{H}_2\text{O})_6^-$ potential surface. Note that the two panels use different energy scales. *Ab initio* geometries for each cluster are depicted in Fig. 4. Isomer hex2 is omitted, for reasons discussed in the text.

model, in contrast, places hex4 a full 2 kcal/mol below the true minimum.

Isomer hex2 is omitted from Fig. 8 because at the *ab initio* geometry shown in Fig. 4 [which is a local minimum at the B3LYP/6-31(1+,3+)G* level of theory], this structure is a transition state on the adiabatic ground-state potential surface generated by the polarizable model Hamiltonian, with an imaginary vibrational frequency of $40i \text{ cm}^{-1}$. This transition state lies on a very flat region of the potential energy surface, and with loose optimization convergence thresholds, the geometry optimization using the polarizable model converges to a structure very close to the *ab initio* one shown in Fig. 4, with relative conformational energies that are very close to MP2/CBS benchmarks evaluated at the *ab initio* geometry. With tight convergence thresholds, however, the topmost water molecule (as shown in Fig. 4) flips its hydrogen atoms towards the exterior of the cluster, while the rest of the cluster collapses in order to donate a second hydrogen bond to this AA water molecule, resulting in an AA isomer that is structurally very similar to hex5. The relative energetics of this new isomer are nearly identical to those of isomer hex5.

C. Pseudopotentials

A direct comparison between the TB potential and our new potential is made in Fig. 9. Because the polarization potential in our model is a many-body effect (and therefore cannot be plotted as a simple one-dimensional potential), both potentials in Fig. 9 are plotted sans polarization, i.e., we omit $V_{\text{pol}}^{\text{TB}}$ [Eq. (6)] from the TB potential, and set all induced dipoles to zero in our model.

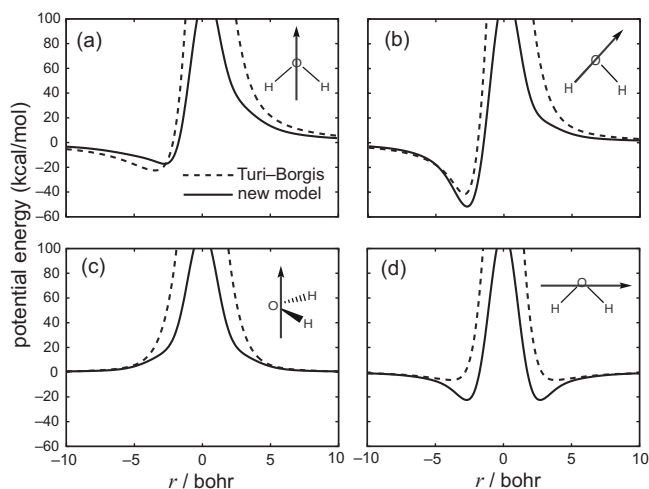


FIG. 9. Comparison of the TB model (dashed curves) and the new potential (solid curves) for H_2O^- , in four one-dimensional slices. To facilitate the comparison, both potentials are shown without polarization. In (a)–(c), $r=0$ represents the H_2O center of mass, whereas in (d), $r=0$ at the oxygen atom.

Compared to the TB potential, our potential is much softer around the oxygen atom and is largely attractive along the in-plane axis perpendicular to the molecular \hat{C}_2 axis [see Fig. 9(d)]. This attraction is a manifestation of the exchange interaction that is implicitly included in the fit. Turi *et al.*¹⁰ showed that a Slater-type (or $X\alpha$ -type) exchange potential⁴⁹

$$V_{X\alpha}(\vec{r}) = -\frac{2}{\pi}k_F(\vec{r}) = -\frac{2}{\pi}[3\pi^2\rho(\vec{r})]^{1/3}, \quad (38)$$

in which $\rho(\vec{r})$ is the electron density of neutral H_2O , reproduces the eigenvalue of the excess electron in the SE approximation. The collection of constants in Eq. (38) corresponds to a Slater-exchange scaling parameter of 1.33, which is larger than the values typically employed in atomic $X\alpha$ calculations,⁴⁹ but consistent with variationally optimized values determined recently for small molecules.⁸⁸

Figure 10 depicts the pseudopotential energy surface for H_2O^- that is obtained using the exchange potential in Eq. (38) scaled by a constant c_x , with $0 \leq c_x \leq 1$. Increasing c_x deepens the potential wells—especially around the oxygen atom—and narrows the repulsive part of the potential. Also note that the difference in well depth between the bisector coordinate in Fig. 10(a) and the bond coordinate in Fig. 10(b) increases with increasing exchange. Although we attempted to adjust the parameters in our potential to fit the numerical pseudopotential surface directly, the results were unsatisfactory; while we were able to reproduce the VEBE of $(\text{H}_2\text{O})_2^-$, we were not able to reproduce the VEBE of even a small number of other structures, based on comparison to MP2 benchmarks.^{40,63,75} TB were similarly unable to achieve a satisfactory direct fit of the pseudopotential energy surface,¹¹ which may indicate an inadequacy in the simple local exchange functional of Eq. (38).

Our new potential model is more attractive along the O–H bond than is the TB model [see Fig. 9(b)], but less attractive along the H–O–H bisector coordinate [Fig. 9(a)]. Perhaps most importantly, we observe that our potential de-

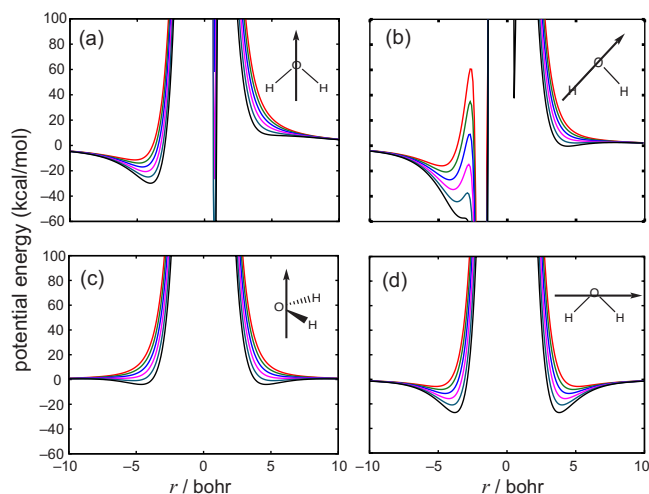


FIG. 10. (Color online) Plots of the pseudopotential for H_2O^- using various $X\alpha$ -type exchange potentials of the form $V_x(\vec{r}) = c_x V_{X\alpha}(\vec{r})$, where $V_{X\alpha}$ is defined in Eq. (38). Values of the scaling parameter c_x range from $c_x=0$ (the top curve, in red, which is least attractive) to $c_x=1$ (the bottom curve, in black, which is most attractive), in increments of 0.2. In (a)–(c), $r=0$ represents the H_2O center of mass, whereas in (d), $r=0$ at the oxygen atom.

cays more rapidly than that of Turi and Borgis [Figs. 9(c) and 9(d)]. This is due to the fact that at long range, the monopole term dominates the electrostatic expansion, and the exaggerated point charges of the SPC model ($q^{\text{O}} = -0.82$, $q^{\text{H}} = 0.41$) provide a more attractive potential than those of AMOEBA ($q^{\text{O}} = -0.51966$, $q^{\text{H}} = 0.25983$). This is significant because the hydrated electron is quite diffuse, and thus the long-range part of the potential is sampled extensively.

D. Energy decompositions

In an effort to understand why our new potential is less repulsive than the TB potential, and also to investigate which $(\text{H}_2\text{O})_n^-$ structures are most affected by polarization, we next examine the expectation values of various components of the electron-water interaction potential, for the same library of $(\text{H}_2\text{O})_n^-$ isomers that was used to evaluate VEBEs. Recall that this library consists of 91 cluster geometries ranging in size from $n=3$ to $n=35$, including both surface states and cavity states. Figures 11–15 show histograms of various expectation values, binned over this library of structures. For ease of analysis, we have subdivided the database into AA-type isomers, non-AA surface states (denoted simply as “surface states” in the discussion that follows), and cavity states.

The histograms in Fig. 11 show the distribution of values for $\langle V_{\text{rep}} \rangle$, the expectation value of the repulsive potential, for both the new model and the TB model. This quantity is smallest, on average, for AA isomers and largest for cavity states, indicating that electron penetration into the molecular core is greatest for cavity states; in AA isomers, the excess electron resides largely outside of the cluster and samples little of the repulsive potential. The most noticeable difference between our model and the TB model is that the latter predicts much larger values of $\langle V_{\text{rep}} \rangle$ in the case of cavity-bound electrons. According to our model, $\langle V_{\text{rep}} \rangle$

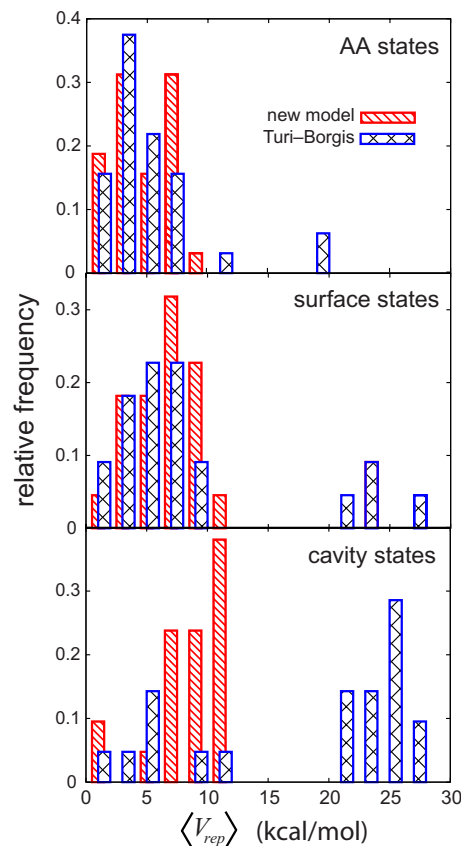


FIG. 11. (Color online) Histograms of the average repulsion energy, for a library of $(\text{H}_2\text{O})_n^-$ isomers.

< 12 kcal/mol for all of the structures in the data set, whereas the TB model affords $\langle V_{\text{rep}} \rangle > 20$ kcal/mol for most cavity states.

Because both models exhibit qualitatively similar VEBEs, the large disparity in $\langle V_{\text{rep}} \rangle$ for cavity states indicates that some other component of the potential must approximately offset this difference. Polarization energy is an obvious candidate. Figure 12 shows a histogram of the quantity

$$\Delta V_{\text{pol}}^{\text{MM}} = \langle V_{\text{pol}}^{\text{MM}} \rangle_{\text{anion}} - \langle V_{\text{pol}}^{\text{MM}} \rangle_{\text{neutral}} \quad (39)$$

for the polarizable model developed here. The notation $\langle \dots \rangle_{\text{anion}}$ and $\langle \dots \rangle_{\text{neutral}}$ indicates whether the dipoles are induced using the electric field for the anionic or the neutral cluster. As our database consists of anion geometries, the quantity $\Delta V_{\text{pol}}^{\text{MM}}$ represents the change in the water-water polarization energy when an electron is added to a water cluster that has already been assembled into its anion geometry. Thus, $\Delta V_{\text{pol}}^{\text{MM}}$ is a reflection of how the inducible dipoles change in response to the electron, and for cavity states we observe a significant increase in the water-water potential upon electron attachment. This increase compensates for a comparatively small repulsive potential.

Note that $\Delta V_{\text{pol}}^{\text{MM}} > 0$ since the induced dipoles computed for the neutral cluster minimize the potential energy of the neutral system, so introduction of the electron must lead to an increase in the water-water part of the potential. The results in Fig. 12 demonstrate that this increase is much larger for cavity states than it is for either AA or surface states, a point to which we shall return.

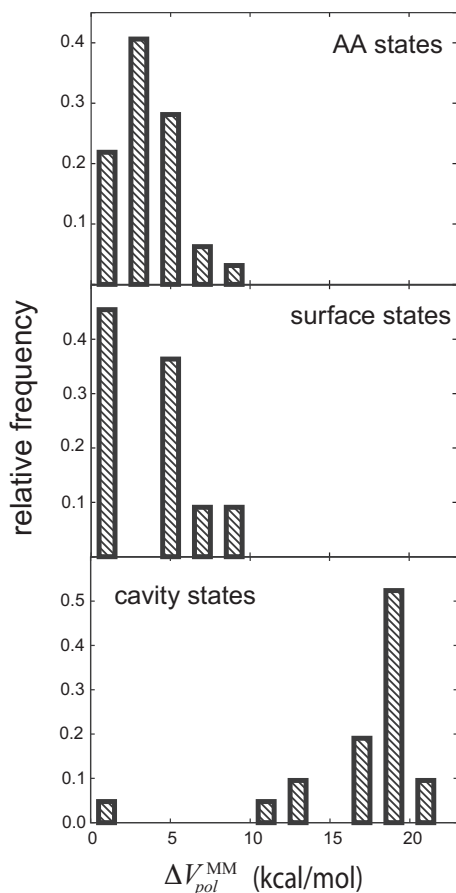


FIG. 12. Histograms illustrating the change in the polarization energy of the water molecules when an electron is added to a water cluster assembled in its anion geometry, as defined in Eq. (39). Expectation values are binned over a library of $(\text{H}_2\text{O})_n^-$ isomers. Results are shown only for the polarizable model.

The pairwise electron-water polarization potential $V_{\text{pol}}^{\text{TB}}$ simulates the effect of the electron polarizing the water molecules, but omits explicit water-water polarization, which is instead included *implicitly* by virtue of fixed SPC point charges that are parametrized for bulk water. In our model, polarization is a many-body effect, and in order to isolate electron-water polarization we must separate out the water-water contribution to the polarization energy. We therefore define the electron-water polarization energy (for our model only) as

$$E_{\text{pol}}^{\text{elec-water}} = E_{\text{pol}} - \langle V_{\text{pol}}^{\text{elec}} \rangle_{\text{neutral}}, \quad (40)$$

where

$$E_{\text{pol}} = \langle V_{\text{pol}}^{\text{elec}} \rangle_{\text{anion}} + W_{\text{pol}}^{\text{elec}} \quad (41)$$

is the total polarization energy, including the polarization work. The quantity E_{pol} is simply the expectation value of the polarization potential defined in Sec. III C, whereas the quantity $\langle V_{\text{pol}}^{\text{elec}} \rangle_{\text{neutral}}$ that we subtract in Eq. (40) represents the average of the electron-induced-dipole interaction, evaluated using the anionic wave function but with dipoles that are converged for the neutral cluster. Thus, $E_{\text{pol}}^{\text{elec-water}}$ is the electronic reorganization energy for introducing an electron into the neutral system. Although E_{pol} is strictly negative (since polarization is variational in our formalism), $E_{\text{pol}}^{\text{elec-water}}$

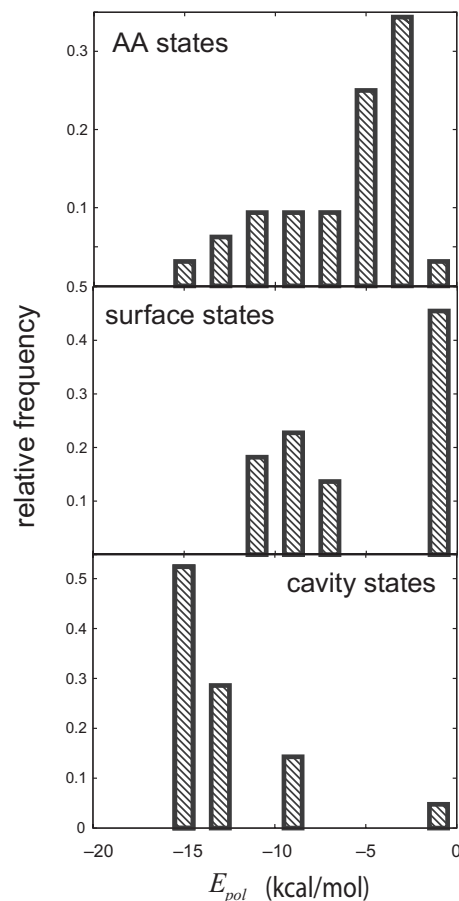


FIG. 13. Histogram of the total polarization energy, as defined in Eq. (41), binned over a library of $(\text{H}_2\text{O})_n^-$ isomers. Results are shown only for the polarizable model developed here.

may have either sign, although in practice it is almost always negative as well.

Figures 13 and 14 show the distribution of values for E_{pol} and $E_{\text{pol}}^{\text{elec-water}}$, respectively, over our database of isomers. The polarization energy is ill-defined for the TB model since the SPC point charges are parametrized for bulk water and therefore implicitly include the effects of water-water polarization; as such, no TB results are presented in Fig. 13. The electron-water polarization energy for the TB model, on the other hand, is simply $E_{\text{pol}}^{\text{elec-water}} = \langle V_{\text{pol}}^{\text{TB}} \rangle$, so Fig. 14 does present a comparison of electron-water polarization for the two models.

Our model tends toward more negative values of the total polarization energy for cavity states than for AA or surface states (Fig. 13), indicating that polarization effects are more important for cavity states. Comparison to Fig. 14 reveals that most of the polarization energy in the cavity states is electron-water polarization, whereas a substantial fraction of E_{pol} for the AA and surface states is water-water polarization. Water networks that support surface-bound isomers of $(\text{H}_2\text{O})_n^-$ (including AA isomers) possess dipoles that are oriented in essentially the same way in both the neutral and the anionic cluster, since it is these dipoles that are ultimately responsible for the fact that the electron is bound. Polarization may certainly amplify electron binding in these isomers, but it does not qualitatively change the electrostatic

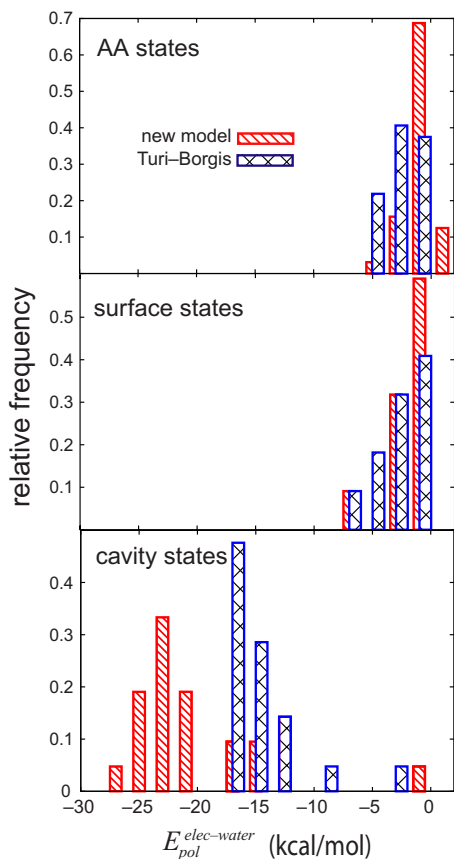


FIG. 14. (Color online) Histogram of the electron-water polarization energy binned over a library of $(\text{H}_2\text{O})_n^-$ isomers. For the TB model, $E_{\text{pol}}^{\text{elec-water}} = \langle V_{\text{pol}}^{\text{TB}} \rangle$, whereas for the polarizable model, $E_{\text{pol}}^{\text{elec-water}}$ is defined in Eq. (40).

environment of the cluster. In cavity-type geometries, on the other hand, the electrostatic environment changes qualitatively when an electron is introduced into the system, resulting in large (in magnitude) values of $E_{\text{pol}}^{\text{elec-water}}$.

There is no way for the simple, distance-dependent polarization model $V_{\text{pol}}^{\text{TB}}$ to capture this distinction. Although the polarizable and nonpolarizable models predict quite comparable values of $E_{\text{pol}}^{\text{elec-water}}$ for AA and surface states (Fig. 14), in the case of cavity states, the polarizable model affords values of $E_{\text{pol}}^{\text{elec-water}}$ that are substantially more negative than those obtained from the TB model. The more negative values obtained with the polarizable model are a manifestation of the compact nature of the wave function in cavity states, which places a large electric field nearby a large number of water molecules, as opposed to a diffuse, surface-bound wave function. This electric field apparently induces dipoles that, in turn, produce a much more attractive potential than the simple $-\alpha/r^4$ polarization potential of TB.

Figure 15 compares $E_{\text{pol}}^{\text{elec-water}}$, the electron-water polarization energy, to $\langle V_{\text{pol}}^{\text{elec}} \rangle_{\text{neutral}}$, the polarization energy in the field of the neutral dipoles. [The sum of these two quantities equals the total polarization energy, according to Eq. (41).] For AA and surface states, the interaction of the electron with the induced dipoles is nearly the same whether the dipoles are converged self-consistently for the anion or simply taken from a neutral cluster calculation at the same geometry. For cavity states on the other hand, the electron-water polar-

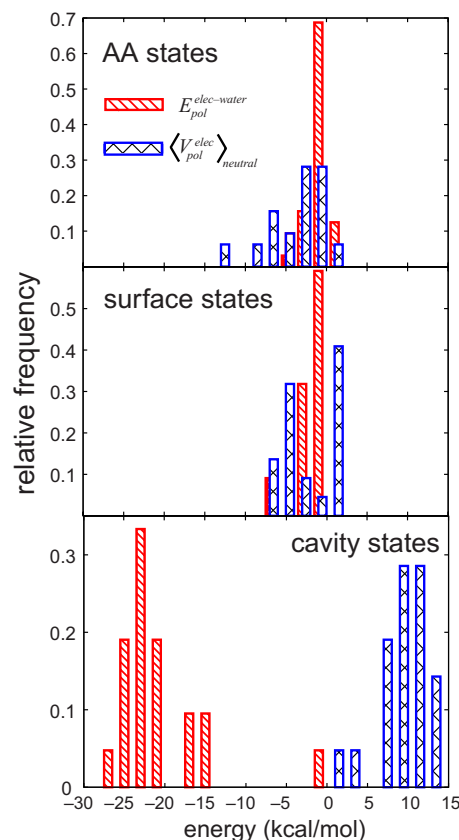


FIG. 15. (Color online) Histogram of the components of the electron-water polarization energy for the polarizable model developed here, binned over a library of $(\text{H}_2\text{O})_n^-$ isomers. The quantities $E_{\text{pol}}^{\text{elec-water}}$ and $\langle V_{\text{pol}}^{\text{elec}} \rangle_{\text{neutral}}$ are the total polarization energy and the polarization energy in the field of the neutral dipoles, respectively.

ization energy (dipoles converged self-consistently for the anion) is large in magnitude and negative in sign, whereas $\langle V_{\text{pol}}^{\text{elec}} \rangle_{\text{neutral}}$ is equally large but positive.

It is perhaps counterintuitive that the electron-water polarization energy should be so much more stabilizing in cavity-type isomers than it is in AA isomers since the latter are characterized by an unpaired electron that is strongly localized around the AA water molecule, which is effectively “buried” within the excess-electron wave function (see, for example, figures in Refs. 43, 84, and 85). This observation is rather revealing, however. Stable surface-bound isomers (including AA isomers) owe their existence to the fact that the water network can reorient to form structures with large dipole moments. In these isomers, the “permanent” (although geometry-dependent) electrostatics, rather than electron-induced polarization, determines the VEBE, as evidenced by the fact that the electrostatic environment of the water cluster is only mildly perturbed by introduction of the electron. Cavity-type isomers, on the other hand, exhibit significant repolarization due to the electron, which is likely a consequence of the more diffuse nature of surface-bound electrons. While permanent electrostatics may suffice to describe surface states, a non-polarizable model may not be able to offer a *balanced* description of both surface and cavity isomers.

We should emphasize that the preceding discussion focuses on just one component of the total reorganization en-

ergy associated with electron attachment, namely, the electronic or noninertial component. Because we employ cluster geometries optimized on the anion potential surface (or extracted from a MD simulation on the anion potential surface), we omit any discussion of orientational reorganization or the dynamics of the electron attachment process. For surface states, the orientational component clearly dominates the electronic component, although the picture is less clear for cavity states. While one might suspect orientational reorganization to be adequately described using fixed-charge potentials, geometry optimizations indicate that the SPC/TB models tend to exaggerate the alignment of molecular dipoles in anionic clusters, and may therefore overestimate orientational reorganization. Because our model can describe both stable neutral clusters and stable anionic clusters, it would seem to be the appropriate tool to address this issue, via direct simulation of the cluster dynamics following electron attachment. We hope to explore this in future simulations.

VII. CONCLUSIONS

We have developed a new electron-water pseudopotential, parametrized for use with the polarizable AMOEBA water model. The result is a one-electron model Hamiltonian from which an electron-water polarization potential arises naturally, and need not be grafted onto the model *a posteriori*. Because we treat electron-water and water-water polarization self-consistently, the model is fully variational and analytic energy gradients are available.

We have constructed our electron-water pseudopotential by following, as closely as possible, the prescription laid out by Turi and co-workers,^{10,11} which is itself based partly on earlier work by Schnitker and Rosicky.⁴ The nonpolarizable TB model¹¹ has been used extensively in the most recent generation of hydrated-electron simulations,^{11,28-32} and it is therefore interesting to compare the performance of this model to one in which the electron-water interaction potential has a very similar form, but where the underlying, polarizable water model is much more accurate. Whereas the TB model is parametrized for the bulk aqueous electron, our pseudopotential is parameterized using the VEBE of $(\text{H}_2\text{O})_n^-$. The new model reproduces *ab initio* benchmarks, for both VEBEs and relative conformational energies, across a diverse set of $(\text{H}_2\text{O})_n^-$ cluster isomers. In particular, the accuracy of VEBEs appears to be fairly insensitive to cluster geometry, leading us to conclude that the description of VEBEs is fairly uniform across the global $(\text{H}_2\text{O})_n^-$ potential surface.

The polarizable model incorporates the fact that introduction of an excess electron must increase the water-water potential energy (even for geometries that exhibit large VEBEs), an effect that is absent in nonpolarizable models. We find that polarization is especially important for cavity states of the excess electron. This result sheds light upon an earlier MP2 study of $(\text{H}_2\text{O})_n^-$ clusters,⁴⁰ where it was found that cavity states exhibit significantly larger correlation energies than surface states, for a given cluster size, even for surface states that possess large VEBEs. Examination of

these same cluster isomers using our polarizable model Hamiltonian suggests that most of this additional correlation energy is polarization rather than dispersion. While a QM treatment of electron-water dispersion (via Drude oscillators^{12,13}) does provide more accurate VEBEs than those obtained with our polarizable model Hamiltonian, such an approach is also considerably more expensive than the present one, and it is not yet clear whether such a treatment is necessary for large, strongly bound cluster anions.

For bulk-like structures exhibiting VEBEs around 2.5 eV (the largest VEBEs in the *ab initio* database that we use for benchmarking), the nonpolarizable TB model (which was parameterized using bulk data¹¹) appears to be slightly more accurate than the new model for prediction of VEBEs. Unfortunately, the paucity of *ab initio* data in this regime makes it difficult to investigate this issue in detail at the present time. In future studies, we shall investigate the properties of the bulk aqueous electron, as predicted by the new model.

ACKNOWLEDGMENTS

This work was supported by the American Chemical Society's Petroleum Research Fund, by a National Science Foundation CAREER award (CHE-0748448), and by an allocation from the Ohio Supercomputer Center. The Visual Molecular Dynamics program⁸⁹ was used for visualization.

- ¹C. D. Jonah, C. Romero, and A. Rahman, *Chem. Phys. Lett.* **123**, 209 (1986).
- ²A. Wallqvist, D. Thirumalai, and B. J. Berne, *J. Chem. Phys.* **85**, 1583 (1986).
- ³A. Wallqvist, D. Thirumalai, and B. J. Berne, *J. Chem. Phys.* **86**, 6404 (1987).
- ⁴J. Schnitker and P. J. Rosicky, *J. Chem. Phys.* **86**, 3462 (1987).
- ⁵R. N. Barnett, U. Landman, and C. L. Cleveland, *Phys. Rev. Lett.* **59**, 811 (1987).
- ⁶R. N. Barnett, U. Landman, C. L. Cleveland, and J. Jortner, *J. Chem. Phys.* **88**, 4421 (1988).
- ⁷A. Staib and D. Borgis, *J. Chem. Phys.* **103**, 2642 (1995).
- ⁸A. Mosyak, P. Graf, I. Benjamin, and A. Nitzan, *J. Phys. Chem. A* **101**, 429 (1997).
- ⁹I. Park, K. Cho, S. Lee, K. S. Kim, and J. D. Joannopoulos, *Comput. Mater. Sci.* **21**, 291 (2001).
- ¹⁰L. Turi, M.-P. Gaigeot, N. Levy, and D. Borgis, *J. Chem. Phys.* **114**, 7805 (2001).
- ¹¹L. Turi and D. Borgis, *J. Chem. Phys.* **117**, 6186 (2002).
- ¹²F. Wang and K. D. Jordan, *J. Chem. Phys.* **116**, 6973 (2002).
- ¹³T. Sommerfeld and K. D. Jordan, *J. Phys. Chem. A* **109**, 11531 (2005).
- ¹⁴A. DeFusco, T. Sommerfeld, and K. D. Jordan, *Chem. Phys. Lett.* **455**, 135 (2008).
- ¹⁵T. Sommerfeld, A. DeFusco, and K. D. Jordan, *J. Phys. Chem. A* **112**, 11021 (2008).
- ¹⁶J. E. Aremu-Cole, Ph.D. thesis, Clemson University, 2007.
- ¹⁷A. Wallqvist, G. Martyna, and B. J. Berne, *J. Phys. Chem.* **92**, 1721 (1988).
- ¹⁸J. Schnitker and P. J. Rosicky, *J. Chem. Phys.* **86**, 3471 (1987).
- ¹⁹R. N. Barnett, U. Landman, C. L. Cleveland, and J. Jortner, *J. Chem. Phys.* **88**, 4429 (1988).
- ²⁰R. N. Barnett, U. Landman, D. Scharf, and J. Jortner, *Acc. Chem. Res.* **22**, 350 (1989).
- ²¹M. Skorobogatiy, I. J. Park, and J. D. Joannopoulos, *Comput. Mater. Sci.* **32**, 96 (2005).
- ²²B. J. Schwartz and P. J. Rosicky, *J. Chem. Phys.* **101**, 6902 (1994).
- ²³B. J. Schwartz and P. J. Rosicky, *J. Chem. Phys.* **101**, 6917 (1994).
- ²⁴C. Nicolas, A. Boutin, B. Levy, and D. Borgis, *J. Chem. Phys.* **118**, 9689 (2003).
- ²⁵F. Wang and K. D. Jordan, *J. Chem. Phys.* **119**, 6973 (2003).

- ²⁶T. Sommerfeld and K. D. Jordan, *J. Am. Chem. Soc.* **128**, 5828 (2006).
- ²⁷T. Sommerfeld, S. D. Gardner, A. DeFusco, and K. D. Jordan, *J. Chem. Phys.* **125**, 174301 (2006).
- ²⁸L. Turi, Á. Madarász, and P. J. Rossky, *J. Chem. Phys.* **125**, 014308 (2006).
- ²⁹D. Borgis, P. J. Rossky, and L. Turi, *J. Chem. Phys.* **125**, 064501 (2006).
- ³⁰D. Borgis, P. J. Rossky, and L. Turi, *J. Chem. Phys.* **127**, 174508 (2007).
- ³¹Á. Madarász, P. J. Rossky, and L. Turi, *J. Chem. Phys.* **126**, 234707 (2007).
- ³²L. Turi, W.-S. Sheu, and P. J. Rossky, *Science* **309**, 914 (2005).
- ³³J. R. R. Verlet, A. E. Bragg, A. Kammrath, O. Cheshnovsky, and D. M. Neumark, *Science* **307**, 93 (2005).
- ³⁴J. R. R. Verlet, A. E. Bragg, A. Kammrath, O. Cheshnovsky, and D. M. Neumark, *Science* **310**, 1769 (2005).
- ³⁵J. V. Coe, S. T. Arnold, J. G. Eaton, G. H. Lee, and K. H. Bowen, *J. Chem. Phys.* **125**, 014315 (2006).
- ³⁶J. V. Coe, S. T. Arnold, J. G. Eaton, G. H. Lee, and K. H. Bowen, *J. Chem. Phys.* **92**, 3980 (1990).
- ³⁷J. V. Coe, *Int. Rev. Phys. Chem.* **20**, 33 (2001).
- ³⁸D. M. Bartels, *J. Chem. Phys.* **115**, 4404 (2001).
- ³⁹T. Frigato, J. VandeVondele, B. Schmidt, C. Schütte, and P. Jungwirth, *J. Phys. Chem. A* **112**, 6125 (2008).
- ⁴⁰C. F. Williams and J. M. Herbert, *J. Phys. Chem. A* **112**, 6171 (2008).
- ⁴¹H. J. C. Berendsen, J. P. M. Postma, W. F. van Gunsteren, and J. Hermans, in *Intermolecular Forces*, edited by B. Pullman (Holland, Dordrecht, 1981), p. 331.
- ⁴²K. Toukan and A. Rahman, *Phys. Rev. B* **31**, 2643 (1985).
- ⁴³J. M. Herbert and M. Head-Gordon, *Proc. Natl. Acad. Sci. U.S.A.* **103**, 14282 (2006).
- ⁴⁴J. M. Herbert, L. D. Jacobson, and C. F. Williams, in *Molecular Potential Energy Surfaces in Many Dimensions*, edited by M. M. Law, J. M. Hutson, J. Tennyson, and A. Ernesti (Collaborative Computational Project on Molecular Quantum Dynamics (CCP6), Daresbury, Warrington, UK, in press).
- ⁴⁵P. Ren and J. W. Ponder, *J. Phys. Chem. B* **107**, 5933 (2003).
- ⁴⁶G. S. Fanourgakis, E. Aprá, and S. S. Xantheas, *J. Chem. Phys.* **121**, 2655 (2004).
- ⁴⁷F. Webster, P. J. Rossky, and R. A. Friesner, *Comput. Phys. Commun.* **63**, 494 (1991).
- ⁴⁸M. A. Morrison and L. A. Collins, *Phys. Rev. A* **17**, 918 (1978).
- ⁴⁹W. Yang and R. G. Parr, *Density Functional Theory of Atoms and Molecules* (Oxford University Press, New York, 1989).
- ⁵⁰G. G. Kleinman and U. Landman, *Phys. Rev. B* **8**, 5484 (1973).
- ⁵¹J. C. Phillips and L. Kleinman, *Phys. Rev.* **116**, 287 (1959).
- ⁵²C. J. Smallwood, R. E. Larsen, W. J. Glover, and B. J. Schwartz, *J. Chem. Phys.* **125**, 074102 (2006).
- ⁵³A. Stone, *Chem. Phys. Lett.* **83**, 233 (1981).
- ⁵⁴A. Stone, *Mol. Phys.* **56**, 1047 (1985).
- ⁵⁵J. Applequist, *Chem. Phys.* **85**, 279 (1984).
- ⁵⁶J. Applequist, *J. Chem. Phys.* **83**, 809 (1985).
- ⁵⁷TINKER, version 4.2, <http://dasher.wustl.edu/tinker>.
- ⁵⁸A. J. Stone, *The Theory of Intermolecular Forces* (Oxford University Press, Oxford, England, 1996).
- ⁵⁹H. Berendsen, J. Grigera, and T. Straatsma, *J. Phys. Chem.* **91**, 6269 (1987).
- ⁶⁰C. J. F. Bottcher, O. V. Belle, P. Bordewijk, and A. Rip, *Theory of Electric Polarization*, Dielectrics in Static Fields, Vol. 1 (Elsevier, New York, 1973).
- ⁶¹B. Thole, *Chem. Phys.* **59**, 341 (1981).
- ⁶²A. DeFusco, D. Schofield, and K. D. Jordan, *Mol. Phys.* **105**, 2681 (2007).
- ⁶³J. M. Herbert and M. Head-Gordon, *J. Phys. Chem. A* **109**, 5217 (2005).
- ⁶⁴M. Dupuis, M. Aida, Y. Kawashima, and K. Hirao, *J. Chem. Phys.* **117**, 1242 (2002).
- ⁶⁵T. H. Choi and K. D. Jordan, *Chem. Phys. Lett.* **464**, 139 (2008).
- ⁶⁶D. Kosloff and R. Kosloff, *J. Comput. Phys.* **52**, 35 (1983).
- ⁶⁷D. T. Colbert and W. H. Miller, *J. Chem. Phys.* **96**, 1982 (1992).
- ⁶⁸J. K. Cullum and R. A. Willoughby, *Lanczos Algorithms for Large Symmetric Eigenvalue Computations* (Birkhauser, Boston, 1985), Vol. 1.
- ⁶⁹C. W. Murray, S. C. Racine, and E. R. Davidson, *J. Comput. Phys.* **103**, 382 (1992).
- ⁷⁰M. L. Leininger, C. D. Sherrill, W. D. Allen, and H. F. Schaefer III, *J. Comput. Chem.* **22**, 1574 (2001).
- ⁷¹Y. Shao, L. F. Molnar, Y. Jung, J. Kussmann, C. Ochsenfeld, S. T. Brown, A. T. B. Gilbert, L. V. Slipchenko, S. V. Levchenko, D. P. O'Neill, R. A. DiStasio, Jr., R. C. Lochan, T. Wang, G. J. O. Beran, N. A. Besley, J. M. Herbert, C. Y. Lin, T. van Voorhis, S. H. Chien, A. Sodt, R. P. Steele, V. A. Rassolov, P. E. Maslen, P. P. Korambath, R. D. Adamson, B. Austin, J. Baker, E. F. C. Byrd, H. Dachsel, R. J. Doerksen, A. Dreuw, B. D. Dunietz, A. D. Dutoi, T. R. Furlani, S. R. Gwaltney, A. Heyden, S. Hirata, C.-P. Hsu, G. Kedziora, R. Z. Khalliulin, P. Klunzinger, A. M. Lee, W. Liang, I. Lotan, N. Nair, B. Peters, E. I. Proynov, P. A. Pieniazek, Y. M. Rhee, J. Ritchie, E. Rosta, C. D. Sherrill, A. C. Simmonett, J. E. Subotnik, H. L. Woodcock III, W. Zhang, A. T. Bell, A. K. Chakraborty, D. M. Chipman, F. J. Keil, A. Warshel, W. J. Hehre, H. F. Schaefer III, J. Kong, A. I. Krylov, P. M. W. Gill, and M. Head-Gordon, *Phys. Chem. Chem. Phys.* **8**, 3172 (2006).
- ⁷²M. A. Rohrdanz and J. M. Herbert, *J. Chem. Phys.* **129**, 034107 (2008).
- ⁷³A. W. Lange, M. A. Rohrdanz, and J. M. Herbert, *J. Phys. Chem. B* **112**, 6304 (2008).
- ⁷⁴R. Kosloff, *J. Phys. Chem.* **92**, 2087 (1988).
- ⁷⁵J. M. Herbert and M. Head-Gordon, *Phys. Chem. Chem. Phys.* **8**, 68 (2005).
- ⁷⁶K. Yagi, Y. Okano, Y. Kawashima, T. Tsuneda, and K. Hirao, *J. Phys. Chem. A* **112**, 9845 (2008).
- ⁷⁷H. Iikura, T. Tsuneda, T. Yanai, and K. Hirao, *J. Chem. Phys.* **115**, 3540 (2001).
- ⁷⁸T. Tsuneda, T. Suzumura, and K. Hirao, *J. Chem. Phys.* **110**, 10664 (1999).
- ⁷⁹ $E_{xc}(\text{BH\&HLYP})=0.5E_x(\text{Becke})+0.5E_x(\text{HF})+E_c(\text{LYP})$.
- ⁸⁰J. C. Rienstra-Kiracofe, G. S. Tschumper, H. F. Schaefer III, N. Sreela, and G. B. Ellison, *Chem. Rev. (Washington, D.C.)* **102**, 231 (2002).
- ⁸¹A. Halkier, T. Helgaker, P. Jørgensen, W. Klopper, and J. Olsen, *Chem. Phys. Lett.* **302**, 437 (1999).
- ⁸²T. Helgaker, P. Jørgensen, and J. Olsen, *Molecular Electronic-Structure Theory* (Wiley, New York, 2000), pp. 322–323.
- ⁸³J. V. Coe, S. M. Williams, and K. H. Bowen, *Int. Rev. Phys. Chem.* **27**, 27 (2008).
- ⁸⁴N. I. Hammer, J. R. Roscioli, and M. A. Johnson, *J. Phys. Chem. A* **109**, 7896 (2005).
- ⁸⁵N. I. Hammer, J. W. Shin, J. M. Headrick, E. G. Diken, J. R. Roscioli, G. H. Weddle, and M. A. Johnson, *Science* **306**, 675 (2004).
- ⁸⁶H. M. Lee, S. Lee, and K. S. Kim, *J. Chem. Phys.* **119**, 187 (2003).
- ⁸⁷J.-W. Shin, N. I. Hammer, J. M. Headrick, and M. A. Johnson, *Chem. Phys. Lett.* **399**, 349 (2004).
- ⁸⁸R. R. Zope and B. I. Dunlap, *J. Chem. Theory Comput.* **1**, 1193 (2005).
- ⁸⁹W. Humphrey, A. Dalke, and K. Schulten, *J. Mol. Graphics* **14**, 33 (1996).